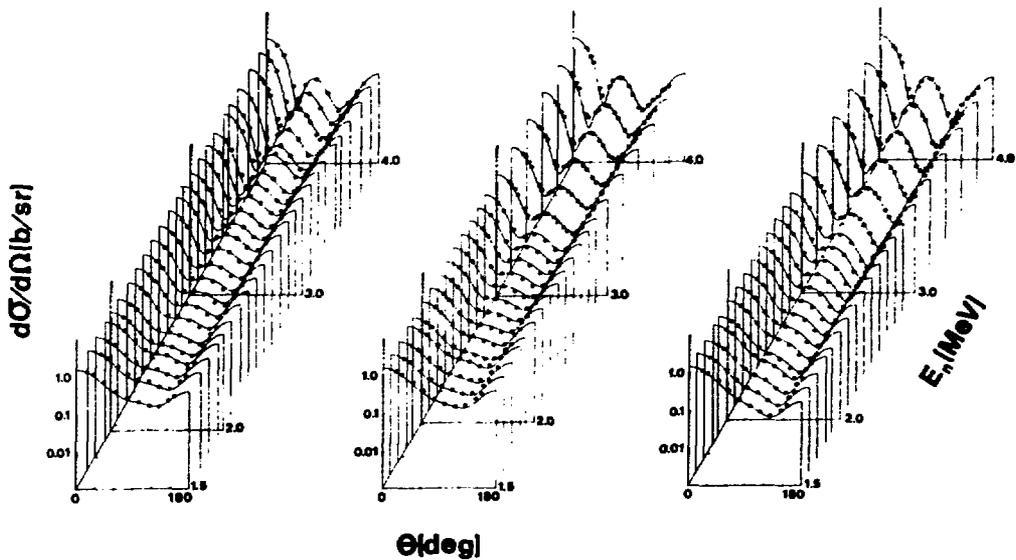# NUCLEAR DATA AND MEASUREMENTS SERIES

ANL/NDM-106

FAST-NEUTRON ELASTIC SCATTERING FROM ELEMENTAL VANADIUM

by

A. B. Smith, P. T. Guenther, and R. D. Lawson

March 1988

ARGONNE NATIONAL LABORATORY, ARGONNE, ILLINOIS

Operated by THE UNIVERSITY OF CHICAGO

for the U. S. DEPARTMENT OF ENERGY

under Contract W-31-109-Eng-38

ANL/NDM-106

FAST-NEUTRON ELASTIC SCATTERING FROM ELEMENTAL VANADIUM[*]

by

A. B. Smith, P. T. Guenther, and R. D. Lawson

March 1988

Keywords

NUCLEAR REACTIONS: Measured $d\sigma/d\Omega(E,\theta)$ for neutrons 4-10 MeV.
Optical-model interpretation.

Applied Physics Division
Argonne National Laboratory
9700 South Cass Avenue
Argonne, Illinois
U. S. A.

NUCLEAR DATA AND MEASUREMENTS SERIES

The Nuclear Data and Measurements Series presents results of studies in the field of microscopic nuclear data. The primary objective is the dissemination of information in the comprehensive form required for nuclear technology applications. This Series is devoted to: a) measured microscopic nuclear parameters, b) experimental techniques and facilities employed in measurements, c) the analysis, correlation and interpretation of nuclear data, and d) the evaluation of nuclear data. Contributions to this Series are reviewed to assure technical competence and, unless otherwise stated, the contents can be formally referenced. This Series does not supplant formal journal publication, but it does provide the more extensive information required for technological applications (e.g., tabulated numerical data) in a timely manner.

Copies on microfiche can be obtained by contacting:

National Technical Information Service
U.S. Department of Commerce
5285 Port Royal Road
Springfield, Virginia 22161
U.S.A.

DISCLAIMER

ANL/NDM-76 Alan B. Smith and Peter T. Guenther, *Scattering of Fast Neutrons from Elemental Molybdenum*, November 1982.

ANL/NDM-77 Donald L. Smith, *A Least-squares Method for Deriving Reaction Differential Cross Section Information from Measurements Performed in Diverse Neutron Fields*, November 1982.

ANL/NDM-78 A.B. Smith, P.T. Guenther and J.F. Whalen, *Fast-neutron Total and Elastic-scattering Cross Sections of Elemental Indium*, November 1982.

ANL/NDM-79 C. Budtz-Joergensen, P. Guenther, A. Smith and J. Whalen, *Few-MeV Neutrons Incident on Yttrium*, June 1983.

ANL/NDM-80 W.P. Poenitz and J.F. Whaler, *Neutron Total Cross Section Measurements in the Energy Region from 47 keV to 20 MeV*, July 1983.

ANL/NDM-81 D.L. Smith and P.T. Guenther, *Covariances for Neutron Cross Sections Calculated Using a Regional Model Based on Elemental-model Fits to Experimental Data*, November 1983.

ANL/NDM-82 D.L. Smith, *Reaction Differential Cross Sections from the Least-squares Unfolding of Ratio Data Measured in Diverse Neutrons Fields*, January 1984.

ANL/NDM-83 J.W. Meadows, *The Fission Cross Sections of Some Thorium, Uranium, Neptunium and Plutonium Isotopes Relative to ^{235}U*, October 1983.

ANL/NDM-84 W.P. Poenitz and J.W. Meadows, *^{235}U and ^{239}Pu Sample-mass Determinations and Intercomparisons*, November 1983.

iv

ANL/NDM-85 D.L. Smith, J.W. Meadows and I. Kanno, *Measurement of the $^{51}V(n,p)^{51}Ti$ Reaction Cross Section from Threshold to 9.3 MeV*, June 1984.

ANL/NDM-86 I. Kanno, J.W. Meadows and D.L. Smith, *Energy-differential Cross-section Measurement for the $^{51}V(n,\alpha)^{48}Sc$ Reaction*, July 1984.

ANL/NDM-87 D.L. Smith, J.W. Meadows, M.M. Bretscher and S.A. Cox, *Cross-section Measurement for the $^{7}Li(n,n't)^{4}He$ Reaction at 14.74 MeV*, September 1984.

ANL/NDM-88 A.B. Smith, D.L. Smith and R.J. Howerton, *An Evaluated Nuclear Data File for Niobium*, March 1985.

ANL/NDM-89 Bernard P. Evain, Donald L. Smith and Paul Lucchese, *Compilation and Evaluation of 14-MeV Neutron-activation Cross Sections for Nuclear Technology Applications: Set I*, April 1985.

ANL/NDM-90 D.L. Smith, J.W. Meadows and P.T. Guenther, *Fast-neutron-spectrum Measurements for the Thick-target $^{9}Be(d,n)^{10}B$ Reaction at $E_d = 7$ MeV*, April 1985.

ANL/NDM-91 A.B. Smith, P.T. Guenther and R.D. Lawson, *On the Energy Dependence of the Optical Model of Neutron Scattering from Niobium*, May 1985.

ANL/NDM-92 Donald L. Smith, *Nuclear Data Uncertainties (Vol.-I): Basic Concepts of Probability*, April 1986.

ANL/NDM-93 D.L. Smith, J.W. Meadows and M.M. Bretscher, *Integral Cross-section Measurements for $^{7}Li(n,n't)^{4}He$, $^{27}Al(n,p)^{27}Mg$, $^{27}Al(n,\alpha)^{24}Na$, $^{58}Ni(n,p)^{58}Co$ and $^{60}Ni(n,p)^{60}Co$ Relative to ^{238}U Neutron Fission in the Thick-target $^{9}Be(d,n)^{10}B$ Spectrum at $E_d = 7$ MeV*, October 1985.

ANL/NDM-94 A.B. Smith, D.L. Smith, P. Rousset, R.D. Lawson and R.J. Howerton, *Evaluated Neutronic Data File for Yttrium*, January 1986.

ANL/NDM-95 Donald L. Smith and James W. Meadows, *A Facility for High-intensity Neutron Irradiations Using Thick-target Sources at the Argonne Fast-neutron Generator*, May 1986.

ANL/NDM-96 M. Sugimoto, A.B. Smith and P.T. Guenther, *Ratio of the Prompt-fission-neutron Spectrum of Plutonium-239 to that of Uranium-235*, September 1986.

ANL/NDM-97 J.W. Meadows, *The Fission Cross Sections of* ^{230}Th, ^{232}Th, ^{233}U, ^{234}U, ^{236}U, ^{238}U, ^{237}Np, ^{239}Pu *and* ^{242}Pu *Relative* ^{235}U *at 14.74 MeV Neutron Energy*, December 1986.

ANL/NDM-98 J.W. Meadows, *The Fission Cross Section Ratios and Error Analysis for Ten Thorium, Uranium, Neptunium and Plutonium Isotopes at 14.74-MeV Neutron Energy*, March 1987.

ANL/NDM-99 Donald L. Smith, *Some Comments on the Effects of Long-range Correlations in Covariance Matrices for Nuclear Data*, March 1987.

ANL/NDM-100 A.B. Smith, P.T. Guenther and R.D. Lawson, *The Energy Dependence of the Optical-model Potential for Fast-neutron Scattering from Bismuth*, May 1987.

ANL/NDM-101 A.B. Smith, P.T. Guenther, J.F. Whalen and R.D. Lawson, *Cobalt: Fast Neutrons and Physical Models*, July 1987.

ANL/NDM-102 D.L Smith, *Investigation of the Influence of the Neutron Spectrum in Determinations of Integral Neutron Cross-Section Ratios*, November 1987.

ANL/NDM-103 A.B. Smith, P. T. Guenther and B. Micklich, *Spectrum of Neutrons Emitted From a Thick Beryllium Target Bombarded With 7 MeV Deuterons*, January 1988.

ANL/NDM-104 L.P. Geraldo and D.L. Smith, *Some Thoughts on Positive Definiteness in the Consideration of Nuclear Data Covariance Matrices*, January 1988

TABLE OF CONTENTS

.

FAST-NEUTRON ELASTIC SCATTERING FROM ELEMENTAL VANADIUM

by

A. B. Smith, P. T. Guenther, and R. ⸱ Lawson

ABSTRACT

Differential neutron elastic- and inelastic-scattering cross sections of vanadium were measured from 4.5 to 10.0 MeV. These results were combined with previous 1.5 to 4.0 MeV data from this laboratory, the 11.1 MeV elastic-scattering results obtained at Ohio University, and the reported neutron total cross sections to energies of ≈ 20.0 MeV, to form a data base which was interpreted in terms of the spherical optical-statistical model. A fit to the data was achieved by making both the strengths and geometries of the optical-model potential energy dependent. This energy dependence was large below ≈ 6.0 MeV. Above ≈ 6.0 MeV the energy dependencies are smaller, and similar to those characteristic of global models. Using the dispersion relationship and the method of moments, the optical-model potential deduced from the 0.0 to 11.1 MeV neutron-scattering data was extrapolated to higher energies and to the bound-state regime. This extrapolation leads to predicted neutron total cross sections that are within 3% of the experimental values throughout the energy range 0.0 to 20.0 MeV. Furthermore, the values of the volume-integral-per-nucleon of the real potential are in excellent agreement with those needed to reproduce the observed binding energies of particle- and hole-states. The latter give clear evidence of the Fermi surface anomaly. Using only the 0.0 to 11.1 MeV data, the predicted E < 0 behavior of the strength and radius of the real shell-model Woods-Saxon potential are somewhat different from those obtained by Mahaux and Sartor in their analysis of nuclei near closed shells. This is attributed to the neglect of higher-energy data in the extrapolation. Because of the dispersion relationship linking the real and imaginary potentials, it is argued that the use of a global optical model for interpreting low-energy data is suspect but, at the same time, probably a reasonable approximation at higher energies.

I. INTRODUCTION

⸱This study of the interaction of fast neutrons with elemental vanadium was motivated by applied and fundamental interests.

Metallic vandium has unusual properties, notably strength at high temperatures and the ability to contain tritium. These characteristics make it an attractive metal in a number of nuclear applications, particularly those associated with the development of fusion-energy systems. For such applications the neutronic properties of vanadium

must be well defined in a comprehensive evaluated nuclear-data file. Such files are constructed from measured quantities, extrapolated and interpolated using nuclear models. An objective of this work was the provision of a quantitative optical model (OM) for use in the formulation of a comprehensive evaluated nuclear-data file reported elsewhere.

In a recent study[1] of neutron interactions with ^{209}Bi, it was found that the characteristic OM potentials changed markedly at $\approx$ 15.0 MeV above the Fermi energy, E_F. At low energies the real radius, r_v (herein all radii are expressed in the form $R_i = r_i \cdot A^{1/3}$), and J_v (the real potential volume-integral-per-nucleon) of the Woods-Saxon potential both decreased rapidly with increasing incident energy, E, whereas the diffuseness of the imaginary Woods-Saxon-derivative interaction, a_w, was small for E $\rightarrow$ 0, and increased rapidly for E $\approx$ 0 to 10.0 MeV. At higher energies, a_w and r_v were essentially energy independent and dJ_v/dE became quite small, approaching a magnitude characteristic of global models.[2,3] This sharp energy dependence of the potential, implied by fitting the neutron total and elastic-scattering cross sections at low energies, had already been observed in earlier work reported from this laboratory.[4,5] Recently an analysis of the 1.5 to 10.0 MeV neutron-scattering data[6] for ^{59}Co exhibited some of the same characteristics as evident in the ^{209}Bi case, with the marked change in the OM parameters occurring $\approx$ 19.0 MeV above E_F. However, the size and energy dependence of the ^{59}Co imaginary potential and other considerations indicated that this nucleus is undoubtedly appreciably deformed. Thus it is of interest to examine a spherical nucleus in the A $\approx$ 50-60 region to see if the OM parameters have an energy dependence and magnitude similar to those obtained for the closed-shell plus-one-proton nucleus ^{209}Bi.

The nucleus ^{51}V ($\approx$ 99.75% elemental abundance) has a closed neutron shell (N = 28) with three valence $f_{7/2}$ protons outside the Z = 20 core. The low-lying excited states observed in this nucleus are very well described in terms of a spherical $(\pi f_{7/2})^3$ shell model.[7] For this reason (and others, as noted later) it was assumed that ^{51}V is a spherical nucleus, and thus the study of neutron scattering from it would test whether or not the OM behavior noted in the A $\approx$ 208 region applied to spherical A $\approx$ 50-60 nuclei. The requisite data base for a quantitative study of the spherical OM of vanadium was obtained by detailed measurements of neutron elastic-scattering cross sections and

selected measurements of inelastic-scattering cross sections at incident energies between 4.5 and 10.0 MeV. These data were extended utilizing neutron scattering and total cross sections for E ≤ 4.0 MeV previously reported from this laboratory,[8,9] the 11.1 MeV elastic-scattering results reported by Ferrer et al,[10] and the neutron total cross sections to 20.0 MeV as given in a recent complementary evaluation.[11]

For spherical nuclei, Mahaux and Sartor[12-15] have used the dispersion relationship connecting the real and imaginary OM potentials,[16] and their moments, to examine the properties of the real interaction at negative energies (i.e., the shell-model potential). In this paper, the OM potential implied by the positive-energy neutron data is examined in the bound-state regime, particularly its capability to predict the single-particle- and hole-state binding energies.

Section II of this paper very briefly outlines the experimental methods employed in the measurements, and the experimental results are presented in Section III. The interpretation of the data base in terms of the spherical optical-statistical model is described in detail in Section IV. Section V presents the implications of the dispersion relations, and Section VI discusses the findings of the work and summarizes the main conclusions.

II. EXPERIMENTAL METHODS

The experimental methods employed in the present neutron-scattering cross-section measurements have been extensively used at the Argonne Tandem Dynamitron. They have been described in detail;[17-19] thus, only a very brief outline is given here.

The measurement samples were fabricated of chemically pure vanadium metal. They were solid cylinders 2 cm in diameter and 2 cm long. The $D(d,n)^3He$ reaction was used as the neutron source throughout the measurements. The source was pulsed at a repetition rate of 2.0 MHz, with a pulse duration of approximately 1 nsec. The incident-neutron energy scale was determined to ± 10 keV by control of the energy of the incident ion beam.

The neutron-scattering measurements were made using the Argonne 10-angle time-of-flight scattering apparatus.[17-20] The time spectra of neutrons scattered over flight paths of ≈ 503 cm were concurrently measured at the ten scattering angles. Two additional time channels provided redundant monitoring of the neutron-source intensity. Relative

detector efficiencies were determined using the spectrum of neutrons emitted from a [252]Cf spontaneously fissioning source.[21] The cross sections were determined relative to the well-known H(n,n) scattering standard.[22] The observed scattering cross sections of vanadium and the reference hydrogen (polyethylene) results were corrected for mulitple-event, incident-beam-attentuation, and angular-resolution effects using the methods of Ref. 23. These procedures involved monte-carlo calculations which were pursued through three iterations.

III. EXPERIMENTAL RESULTS

The elastic-scattering measurements were made at $\approx$ 500 keV intervals from 4.5 to 10.0 MeV. Forty to eighty differential values were obtained at each incident energy, distributed between $\approx$ 18$^{\text{o}}$ and 160$^{\text{o}}$. Incident-neutron resolution decreased from $\approx$ 300 keV at 4.5 MeV to $\approx$ 100 keV at 10.0 MeV. Scattered-neutron resolution was intentionally kept relatively broad so as to assure that scattered neutrons resulting from the excitation of the first, 320 keV, state were included with the elastically-scattered component, while at the same time neutrons due to the excitation of higher-lying levels were excluded.[24] The relative energy sensitivities of each of the time-of-flight detectors, as determined using the [252]Cf fission spectrum, were normalized to an absolute scale by observing neutron scattering from the well-known H(n,n) (polyethylene sample) standard reaction. Relative scattering angles were determined to $\approx$ 0.1$^{\text{o}}$ using conventional optical methods. The absolute calibration of this relative angular system was determined by observing the scattering of neutrons from a heavy target having a very pronounced angular distribution, both left and right of the apparent center line. This procedure provided a zero-degree calibration with an accuracy of $\approx$ ± 0.2$^{\text{o}}$. The measurements were made over a several-year period, in an energy-random manner, using different instrument settings. The consistency of the results was good. In addition, differential elastic-scattering cross sections of carbon, which were measured concurrently with those of vanadium, were in good agreement with the well-known values.[22]

The statistical uncertainties of the differential values varied from < 1%, in regions of large cross sections, to > 10% at the minima of the distributions. Systematic uncertainties, primarily arising from the absolute calibration of the detectors, were estimated to be $\leq$ 3%. Correction procedures introduced additional errors that were generally $\leq$ 1%, except at the minima of the distributions where they could be considerably larger. The above-cited angle calibration implies significant cross-section uncertainty in angular regions of rapidly

varying cross section. Finally, a minimum cross-section sensitivity of ≈ 1.5 mb/sr was subjectively assumed as representative of small errors from unidentified sources. This latter contribution has a negligible effect, except at the very minima of the higher-energy distributions. These various components were combined in quadrature to obtain the total uncertainty.

As illustrated in Fig. 1, the present work nicely extrapolates to the lower-energy results previously reported from this laboratory[9] and to the 11.1 MeV results of Ferrer et al.[10] Using averages at lower energies to smooth fluctuations, the data base of Fig. 1 provides a good foundation for the study of physical models from 1.5 MeV to 11.1 MeV. Illustrative comparisons of the present results with previously reported values are presented in Fig. 2. It is clear from an inspection of the total cross section[11] that considerable fluctuations in the elastic-scattering should be expected up to energies of more than 5.0 MeV. Thus, comparisons of experimental results below incident energies of ≈ 6.0 MeV are sensitive to exact experimental energy scales and resolutions. The comparisons shown in Fig. 2 are relatively good. Other data sets, drawn from the files of the National Nuclear Data Center, compare far less favorably.

The primary goal of the measurements was the above elastic-scattering cross sections. However, some ancillary neutron inelastic-scattering results were obtained for the excitation of the 929 keV level, and for the composite excitation of the 1609 and 1813 keV states. These inelastic-scattering results are compared with some previously reported ones in Fig. 3. Only one set of prior results (Ref. 25) extends to any appreciable extent into the region of the present measurements. In that case, the agreement with the results of the present work is good. At the higher energies of the present work the inelastic-scattering cross sections are small (a few mb/sr), suggesting that the processes are largely of a compound-nucleus nature. However, the values do remain larger than predicted by statistical-model calculations, as discussed below.

IV. INTERPRETATION

The theoretical interpretation was based upon the conventional spherical-optical-statistical model.[35-37] Inherent in this approach is the assumption of a spherical nucleus with only shape and compound-nucleus scattering contributing to the neutron-induced processes. The OM potential was assumed to consist of a real Woods-Saxon, an imaginary Woods-Saxon-derivative, and a Thomas spin-orbit interaction.[36] No volume absorption or imaginary spin-orbit

5
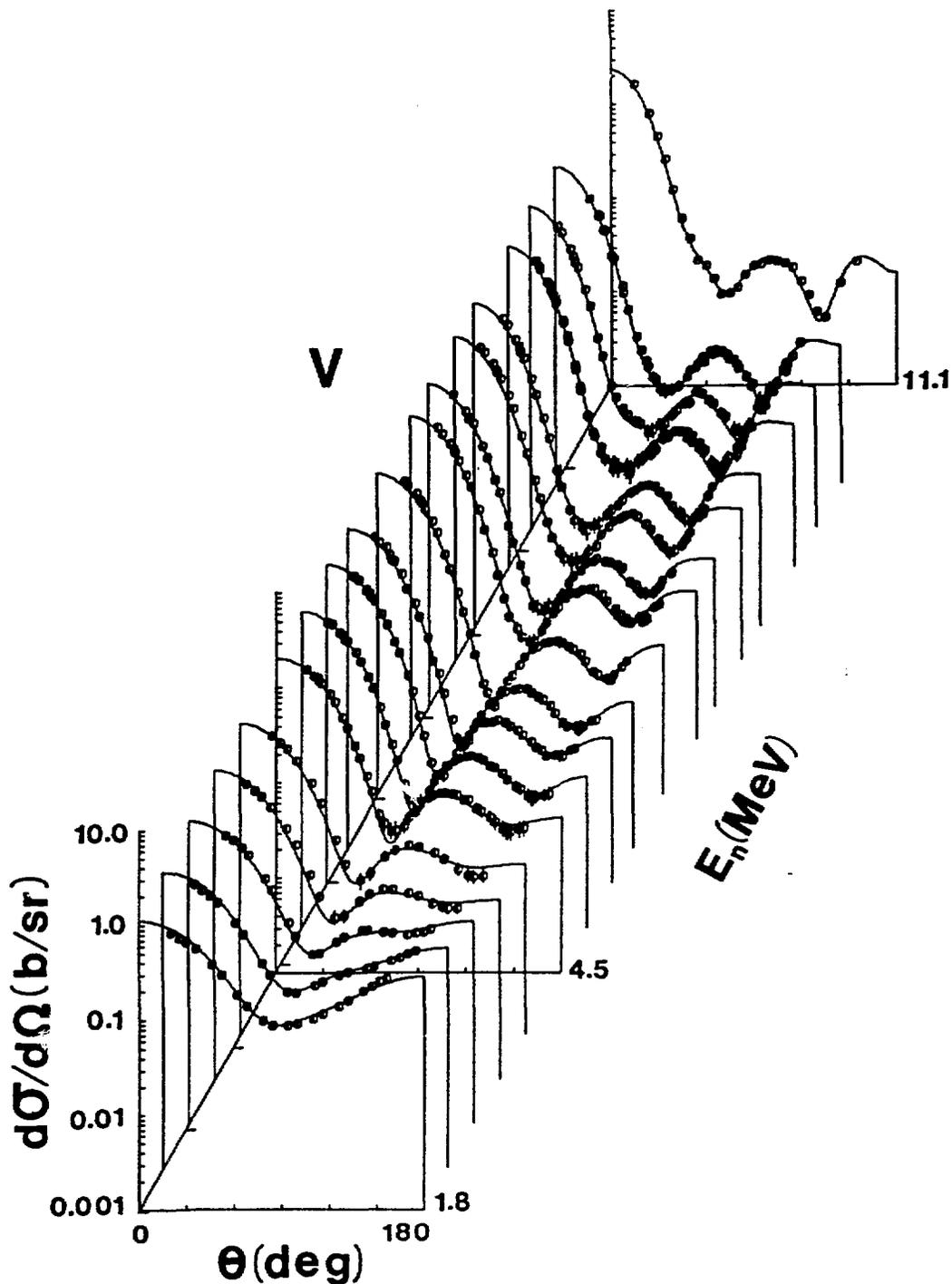
Fig. 1. Differential elastic-scattering cross sections of vanadium. Measured values are indicated by data symbols. Curves are the result of four-parameter fitting, as described in the text. The results over the range 4.5 to 10.0 MeV are from the present work. The 11.1 MeV distribution is from ref. 10. Distributions in the 1.8 to 4.0 MeV range are ≈ 500 keV averages of the results of Ref. 9. The data are shown in the laboratory coordinate system.
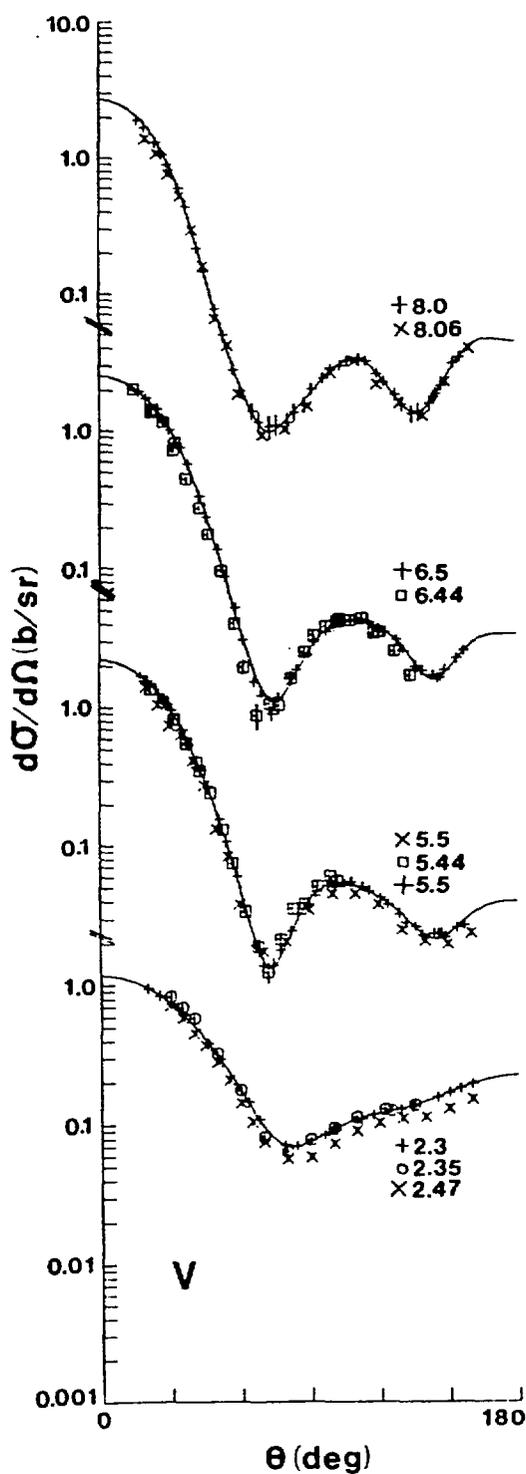
Fig. 2. Selected comparisons of measured differential elastic-scattering cross sections. Symbols indicate measured values as follows: ☐ = Ref. 25, O = Ref. 26, X = Ref. 27 and + = the present work (extended below 4.5 MeV using earlier work from this laboratory[9]). Curves are eye-guides obtained using least-squares legendre-polynomial fitting. The approximate incident-neutron energies are indicated numerically in MeV. The data are given in the laboratory coordinate system.
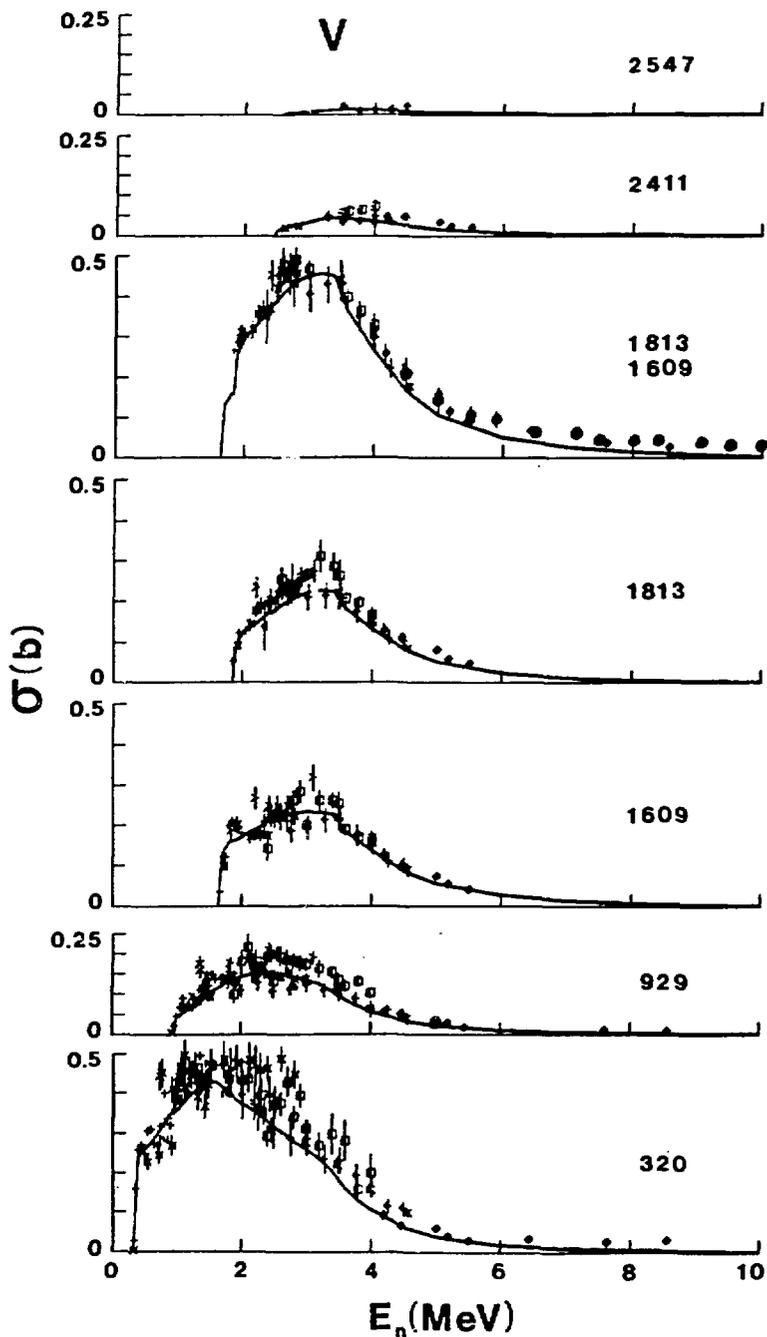
Fig. 3. Illustrative inelastic-neutron-scattering excitation cross sections. The results of the present work are noted by ● symbols. Previously reported values are given by: X = Ref. 8, O = Ref. 9, △ = Ref. 26, + = Ref. 28, ← = Ref. 29, X̄ = Ref. 30, N = Ref. 31, Y = Ref. 32, □ = Ref. 33, and * = Ref. 34. Excitation energies are cited numerically in each portion of the figure in keV. The curves are the results of the statistical-model calculations described in the text.

8

potential was considered, as there is no evidence for their contribution in similar studies in this mass-energy region.[38] All compound-nucleus contributions were calculated from the Hauser-Feshbach formula,[37] as modified for width-fluctuation and correlation corrections by Moldauer,[39] and were carried out using the computer code ABAREX.[40]

The data base used in the interpretation consisted of:

i) The present elastic-scattering results, extending from 4.5 to 10.0 MeV, discussed in Section III.

ii) The 11.1 MeV elastic-scattering distribution reported by Ferrer et al.[10] This measurement was part of an extensive 11.1 MeV study extending over a wide mass range.

iii) The elastic scattering of Ref. 9, averaged over $\approx$ 500 keV incident-energy intervals so as to provide five angular distributions with mean energies of 1.8, 2.3, 2.8, 3.3, and 3.8 MeV. The broad averages are necessary to smooth the obvious fluctuations in the individual experimental angular distributions. A second averaging procedure was also examined in which the individual angular distributions were concurrently fitted within $\approx$ 500 keV energy intervals. The OM parameters obtained using the two different averaging procedures were nearly the same. Thus, although the compound-nucleus contributions undoubtedly change over the averaging interval, there was not a significant effect on the OM parameters in this case. The OM parameters presented later in this Section are those obtained using the first of these two alternative methods, as much less calculational time was involved.

iv) The energy-averaged neutron total cross sections of Ref. 11, extending from $\approx$10.0 keV to 20.0 MeV. Ref. 11 presents a rigorous statistical evaluation of all of the experimental, total cross-section results available from the National Nuclear Data Center.[41]

v) The ℓ = 0 strength function, S_o, deduced from low-energy resonance observations.[42]

No elastic-scattering data has apparently been reported between 11.1 and 20.0 MeV,[43] except a single 14.7 MeV distribution[13] which does

not have the precision and detail desirable for model fitting. There are a few other previously reported elastic-scattering distributions in the 1.5 to 10.0 MeV range, as cited above, but they are only at isolated energies, of variable quality and completness, and frequently not particularly consistent with one another. Therefore, they were not used in the present interpretation. If included, they would have such a low weight that their impact on the resulting parameters would be small. There are previously reported elastic-scattering distributions below 1.5 MeV,[8,45] as a result of work at this laboratory. However, they are subject to very large fluctuations and are not as sensitive to model parameters since they are far more isotropic than the higher-energy distributions. Thus, they were not used in the present interpretation.

Although there is no reason to believe that the measured data on vanadium are of inferior quality, the derivation of the OM parameters from them proved difficult. Indeed, the measurements were generally a part of an extensive experimental program, and results concurrently obtained for other targets have proven very satisfactory.[1,6] Fluctuations are obviously a serious concern to more than 5.0 MeV, even with the relatively broad experimental resolutions of the data averages cited above. The fluctuation problem becomes more acute as the energy decreases. The first excited level of ^{51}V is at 320 keV.[24] Inelastically scattered neutrons associated with the excitation of this level were resolved from the elastically scattered neutrons at incident energies of $\leq$ 4.0 MeV. Above 4.0 MeV, the experimental data included the first inelastic-neutron group with the elastically scattered component, and the calculational procedures combined the two groups when fitting the experimental data. While this approach is sound, it tends to obscure the minima of the elastic distributions, rendering the OM parameters somewhat less precise. Even at the highest energies, the observed distributions were generally structureless compared to those observed in scattering from heavier nuclei. They are characterized by a prominent forward-angle maximum, a single relatively weak secondary maximum at larger angles, and two rather broad and ill-defined minima. Distributions of this nature do not provide the sharp structure characteristic of higher energies, and/or heavier-mass targets, and thus do not lead to well-defined OM parameters.

The model parameters were determined by minimizing χ^2, where

$$\chi^2 = \frac{1}{N} \sum_{1}^{N} \left[\frac{\sigma_i(\exp) - \sigma_i(\text{cal})}{\delta\sigma_i(\exp)} \right]^2 , \tag{1}$$

with $\sigma_i(\exp)$ the ith observable, $\delta\sigma_i(\exp)$ its uncertainty, $\sigma_i(\text{cal})$ the corresponding calculated value, and N the number of data points at the

energy of interest. One value of σ_i may be the value of the total cross section, as discussed below. Primary emphasis was placed upon data obtained at energies ≥ 4.0 MeV where the fluctuations were less pronounced. The fitting procedure included compound-nucleus contributions below 8.0 MeV incident energy. At higher energies it was assumed that the elastic scattering was entirely a "shape" process.

The interpretation is most sensitive to the spin-orbit potential at the higher energies of the present study. It was assumed that the spin-orbit radius was 1.0 fm and the diffuseness was 0.65 fm. These geometric values are consistent with those recently obtained in this mass region[6,38], and with those generally cited in the literature.[36] The spin-orbit potential strength was determined from considerations of the present experimental results for the elastic scattering of 9.0, 9.5, and 10.0 MeV neutrons. Two approaches were used. In the first, a mesh of spin-orbit strengths was taken and the remaining six parameters (real and imaginary strengths, radii and diffusenesses) concurrently fitted, minimizing χ^2. In the second, a reasonable OM was assumed, and the spin-orbit strength alone was fitted. The results of the two methods were very similar, with an average spin-orbit strength of 8.36 MeV. No polarization data suitable for verifying the spin-orbit potential at energies above ≈ 1.0 MeV was located in the literature. All of the subsequent fitting and discussion of this paper assumed this spin-orbit potential,

$$
\begin{aligned}
V_{so} &= 8.36 \quad \text{MeV} \\
r_{so} &= 1.00 \quad \text{fm} \\
a_{so} &= 0.65 \quad \text{fm}.
\end{aligned}
\tag{2}
$$

These values are similar to those deduced at 11.1 MeV by Ferrer et al.[10]

The 26 discrete levels used in the compound-nucleus calculations were taken from Ref. 24. They are listed in Table I, and extend to an excitation energy of ≈ 3.5 MeV. For states above 3.0 MeV the spin assignments are often uncertain, and some states may have been missed. However, below 3.0 MeV the states are well known and they will dominate the compound-nucleus processes at low energies. Above ≈ 3.5 MeV the excited states were represented by a continuum distribution, with the level density given by

$$
\rho(E,J) = \frac{(2J + 1)}{2\sigma^2 T} \cdot \exp((E - E_o)/T) \cdot \exp(-(J + 1/2)^2/2\sigma^2),
\tag{3}
$$

where J is the angular momentum of the continuum target level and E_o, T, and σ are parameters used to describe the higher-energy excitations, and

11

their values were taken from Gilbert and Cameron.[46] The temperature, T, was varied in the fitting procedure for E ≤ 6.5 MeV. The results suggest appreciable fluctuation of T, but in a random manner. Thus E_o, T, and σ were kept fixed at the values of Ref. 46 for the remainder of the fitting.

As noted above, the elastic distributions consist primarily of the prominent forward peak with only modest detail at larger scattering angles. The magnitude of the forward peak is closely related to the neutron total cross section through the optical theorem, and the energy-averaged behavior of the latter is well known from the rigorous experimental evaluation of Ref. 11. Thus the evaluated neutron total cross section, together with the differential elastic-scattering cross sections (generally excluding values forward of 35° to 45°), were used in the fitting procedures. The weights associated with the total cross sections were a factor of ten larger than those of the individual differential elastic-scattering values.

The initial fitting procedures concurrently varied the six parameters, real and imaginary strengths, radii, and diffusenesses. The fits were not constrained and the resulting parameters fluctuated from energy to energy. However, the real radius, r_v, decreased with energy in an approximately linear manner, and the imaginary radius, r_w, followed r_v but was slightly larger. These trends are reasonably represented by

$$r_v = (1.34 - 0.009 \cdot E) \quad fm$$
$$r_w = 1.025 \cdot r_v,$$

(4)

where, throughout this work, E is the incident neutron energy in MeV.

With the radii fixed by Eq. (4), four parameter fits to the data base were made from 1.8 to 11.1 MeV. The resulting parameters led to a very good description of the observed differential elastic scattering, as illustrated by the curves in Fig. 1. The energy dependencies of the resulting parameters are not simple, particularly at the lower energies. However, the real diffuseness, a_v, was essentially energy independent, with an average value of a_v = 0.574 fm. The imaginary diffuseness, a_w, had a broad maximum at ≈ 6.0 MeV, as illustrated by the dashed curve in Fig. 4. Above ≈ 6.0 MeV, a_w decreased with energy to an approximately constant value of ≈ 0.4 fm at 10.0 to 11.0 MeV. The trend of a_w below ≈ 6.0 MeV is somewhat ambiguous. The results in the 3.0 to 4.0 MeV range extrapolate to a relatively large value at zero energy, while

Table I. E_x and J^π values used in the compound-nucleus calculations. The values were taken from Ref. 24.

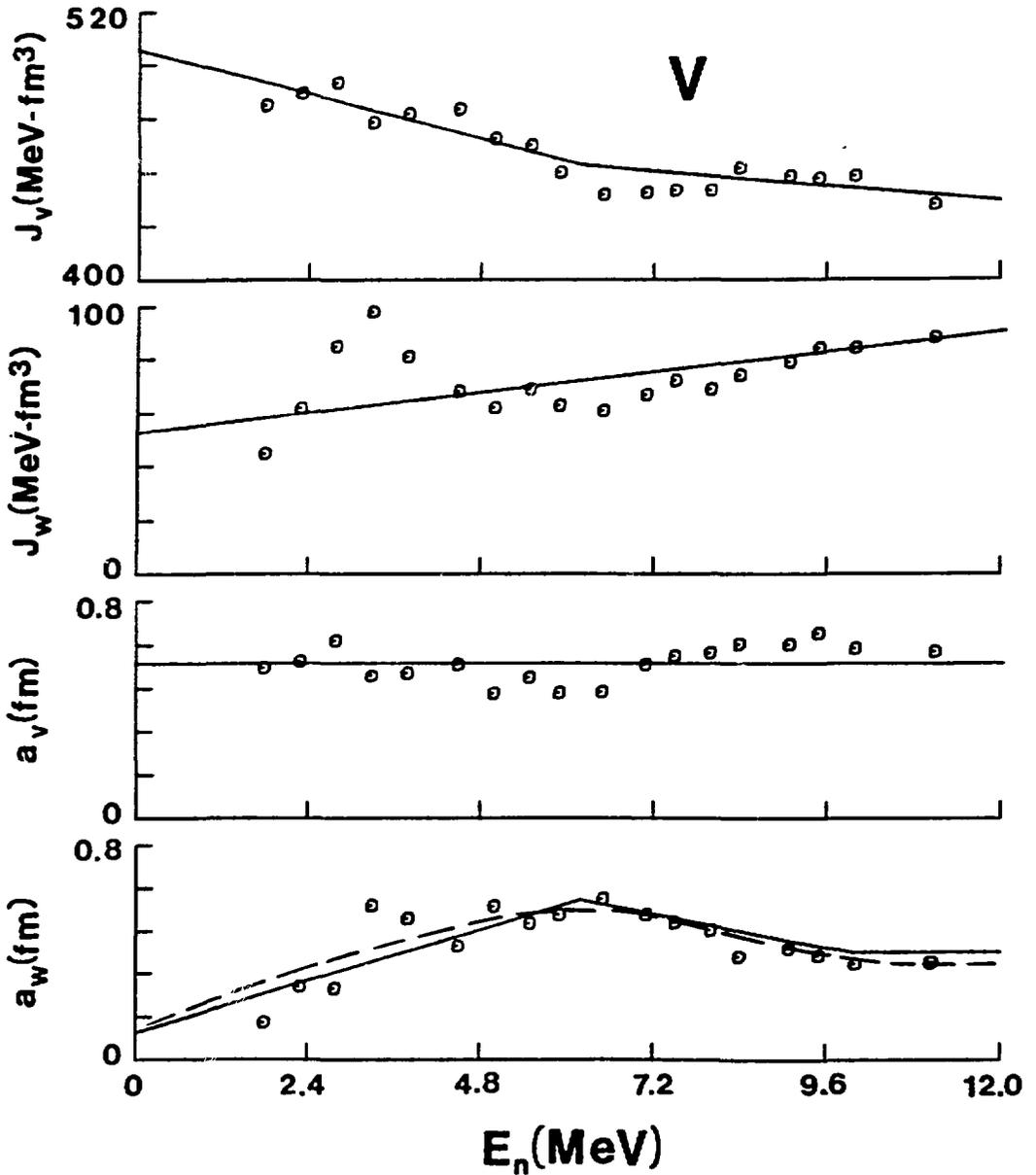| Level No.	E_x (MeV)	J^π values
1	0.0 (g.s.)	$7/2^-$
2	0.320	$5/2^-$
3	0.929	$3/2^-$
4	1.609	$11/2^-$
5	1.813	$9/2^-$
6	2.411	$3/2^-$
7	2.547	$1/2^+$
8	2.677	$3/2^+$
9	2.699	$15/2^-$
10	3.084	$5/2^-$
11	3.150	$3/2^-$
12	3.195	$3/2^-$
13	3.215	$3/2^-$
14	3.264	$5/2^-$
15	3.280	$5/2^+$
16	3.372	$1/2^-$
17	3.377	$5/2^-$
18	3.378	$9/2^-$
19	3.381	$3/2^-$
20	3.383	$9/2^-$
21	3.386	$13/2^-$
22	3.396	$13/2^-$
23	3.444	$3/2^-$
24	3.445	$9/2^-$
25	3.454	$9/2^-$
26	3.517	$5/2^-$

Fig. 4. The volume-integrals-per-nucleon of the real, J_v, and imaginary, J_w, potential strengths and the real, a_v, and imaginary, a_w, potential diffusenesses are shown as a function of energy. The solid curves are the values given by Eq. (7), and the dashed curve an eye-guide, as described in the text.

those obtained at 1.8, 2.3, and 2.8 MeV suggest that a_w becomes small at zero energy. With the radii cited above, the fits to the data in the 3.0 to 4.0 MeV range were not very good, while those at lower energies were quite acceptable. These variations may well be a manifestation of fluctuations in the underlying data. Either extrapolation of a_w to zero energy results in an S_0 strength function close to that derived from resonance data,[42] so S_0 gives very little guidance in this case. However, the energy-averaged neutron total cross section is at a minimum in the 0.5 to 1.0 MeV region and this observation is consistent only with small values of a_w at low energies, as indicated by the dashed curve in Fig. 4. This behavior can be qualitatively approximated by the following linear segments

$$a_w = 0.1 + 0.08 \cdot E \quad \text{fm} \quad (E \leq 6.2 \text{ MeV})$$
$$a_w = 0.92 - 0.052 \cdot E \quad \text{fm} \quad (6.2 \leq E \leq 10.0 \text{ MeV}), \tag{5}$$

illustrated by the solid curves in Fig. 4.

The magnitudes and energy dependencies of the volume integral-per-nucleon of the real, J_v, and imaginary, J_w, potentials are also shown in Fig. 4. (Somewhat similar energy behavior was found for the quantities $V_0 \cdot r_v^2$ and $W_0 \cdot a_w$, where V_0 and W_0 are, respectively, the real and imaginary potential depths.) There is considerable scatter in the values of J_v and J_w, and this increases with decreasing energy, making quantitative interpretation difficult. However, J_w increases approximately linearly with energy, particularly above ≈ 5.0 MeV, whereas J_v decreases with energy, more rapidly below ≈ 6.0 MeV than at higher energies. These strengths are reasonably represented by the functions

$$J_v = (503 - 8.3 \cdot E) \text{ MeV} \cdot \text{fm}^3 \quad E \leq 6.2 \text{ MeV}$$
$$J_v = (470 - 2.9 \cdot E) \text{ MeV} \cdot \text{fm}^3 \quad E \geq 6.2 \text{ MeV} \tag{6}$$
$$J_w = (53 + 3.1 \cdot E) \text{ MeV} \cdot \text{fm}^3.$$

Again, these linear approximations are illustrated by the solid curves in Fig. 4.

Clearly, the linear dependence on E of r_v, r_w, and a_w, given by Eqs. (4) and (5), will lead to trouble at higher energies. If one

requires that the total cross section be fitted to 20.0 MeV, then above ≈ 10.0 MeV these quantities become energy independent and an adequate characterization of the spherical OM potential in the energy range 0.0 to 20.0 MeV is given by

$$J_V = (503 - 8.3 \cdot E) \text{ MeV} \cdot \text{fm}^3 \qquad E \leq 6.2 \text{ MeV}$$

$$J_V = (470 - 2.9 \cdot E) \text{ MeV} \cdot \text{fm}^3 \qquad E \geq 6.2 \text{ MeV}$$

$$r_V = (1.34 - 0.009 \cdot E) \text{ fm} \qquad E \leq 10.0 \text{ MeV}$$

$$r_V = 1.25 \text{ fm} \qquad E \geq 10.0 \text{ MeV}$$

$$a_V = 0.574 \text{ fm}$$

$$\qquad (7)$$

$$J_W = (53 + 3.1 \cdot E) \text{ MeV} \cdot \text{fm}^3$$

$$r_W = 1.025 \cdot r_V$$

$$a_W = (.1 + 0.08 \cdot E) \text{ fm} \qquad E \leq 6.2 \text{ MeV}$$

$$a_W = (0.92 - 0.052 \cdot E) \text{ fm} \qquad 6.2 \leq E \leq 10.0 \text{ MeV}$$

$$a_W = 0.40 \text{ fm} \qquad E \geq 10.0 \text{ MeV}.$$

The specific values given by Eq. (7) do not always give as good a description of the elastic angular distributons as those shown in Fig. 1 because of the large spatter of the potential parameters illustrated in Fig. 4. Furthermore, the linear segments of Eqs. (7) are doubtless only an approximation of a more energy-smooth behavior, as suggested by the dashed line in Fig. 4. However, as shown in Fig. 5A, Eqs. (2) and (7) reproduce the data very well out to the first minimum. In addition, the predicted elastic-scattering distributions below 1.5 MeV, calculated with this parameterization, are in reasonable agreement with a broad energy-average of the experimental data.[8] However, at the very lowest energies, where resonance fluctuations are large and it is doubtful that a true energy-average of the experimental cross sections (in the sense of the OM) has been obtained, calculation and experiment do deviate. Finally, Eq. (7) leads to an S_0 strength function of 7.34×10^{-4}, compared to the value $(7.7 \pm 1.2) \times 10^{-4}$ deduced from resonance data.[42]

In the energy range 0.0 to 20.0 MeV, the total cross section predicted from the OM parameterization of Eqs. (2) and (7) is shown by the "light" curve in Fig. 6. The calculated results are within ≈ 3% of the experimental values and generally well within the spread of the data.

The potential of Eq. (7) leads to the inelastic neutron-scattering excitation functions shown in Fig. 3. The present measurements contributed to the experimental data base above ≈ 4.0 MeV, particularly

16

the prominent excitation of the 1609 ($11/2^-$) and 1813 ($9/2^-$) keV levels, as illustrated. The results of the calculations are generally consistent with the experimental values obtained using direct neutron detection, but somewhat smaller than the results deduced from (n;n',γ) measurements. Many of the latter experimental results were obtained at isolated energies and there are large fluctuations at the lower energies, as illustrated, for example, in Ref. 8. The calculations of inelastic scattering assumed only statistical processes, and they apparently make up a very large majority of the inelastic-scattering cross section. Above ≈ 7.0 MeV, the experimental results, particularly those of the present work, are slightly larger than those calculated with the statistical theory. However, the differences are only a few mb/sr, indicating that any direct-reaction component is very small.

Fluctuations in the underlying data may have distorted some of the OM parameters given in Eq. (7). However, the general trends of the potential appear real, and alternate approaches to the fitting led to qualitatively the same conclusions. Thus, while there remain unavoidable uncertainties in the interpretation, the resulting parameterization is certainly suitable for applied usage.

V. DISPERSION RELATIONS

There is a well known dispersion relationship linking the real and imaginary OM potentials[16]

$$V(r,E) = V_{HF}(r,E) + \frac{P}{\pi} \int_{-\infty}^{+\infty} \frac{W(r,E')}{E - E'} \, dE',\tag{8}$$

where $V(r,E)$ is the total real OM interaction, $V_{HF}(r,E)$ is its Hartree-Fock component, P is the principal-value integral, and $W(r,E)$ is the absorptive potential. The same dispersion relationship holds for the radial moments of the potentials, that is

$$<r(E)^q>_V = <r(E)^q>_{HF} + \frac{P}{\pi} \int_{-\infty}^{+\infty} \frac{<r(E')^q>_W}{E - E'} \, dE',\tag{9}$$

where, for example,

$$<r(E)^q>_W = \frac{4\pi}{A} \int W(r,E) \, r^q \, dr.\tag{10}$$

Mahaux and Sartor[12-14] argue that the energy dependence of the radial moments of $<r(E)^q>_W$ can be parameterized by the form
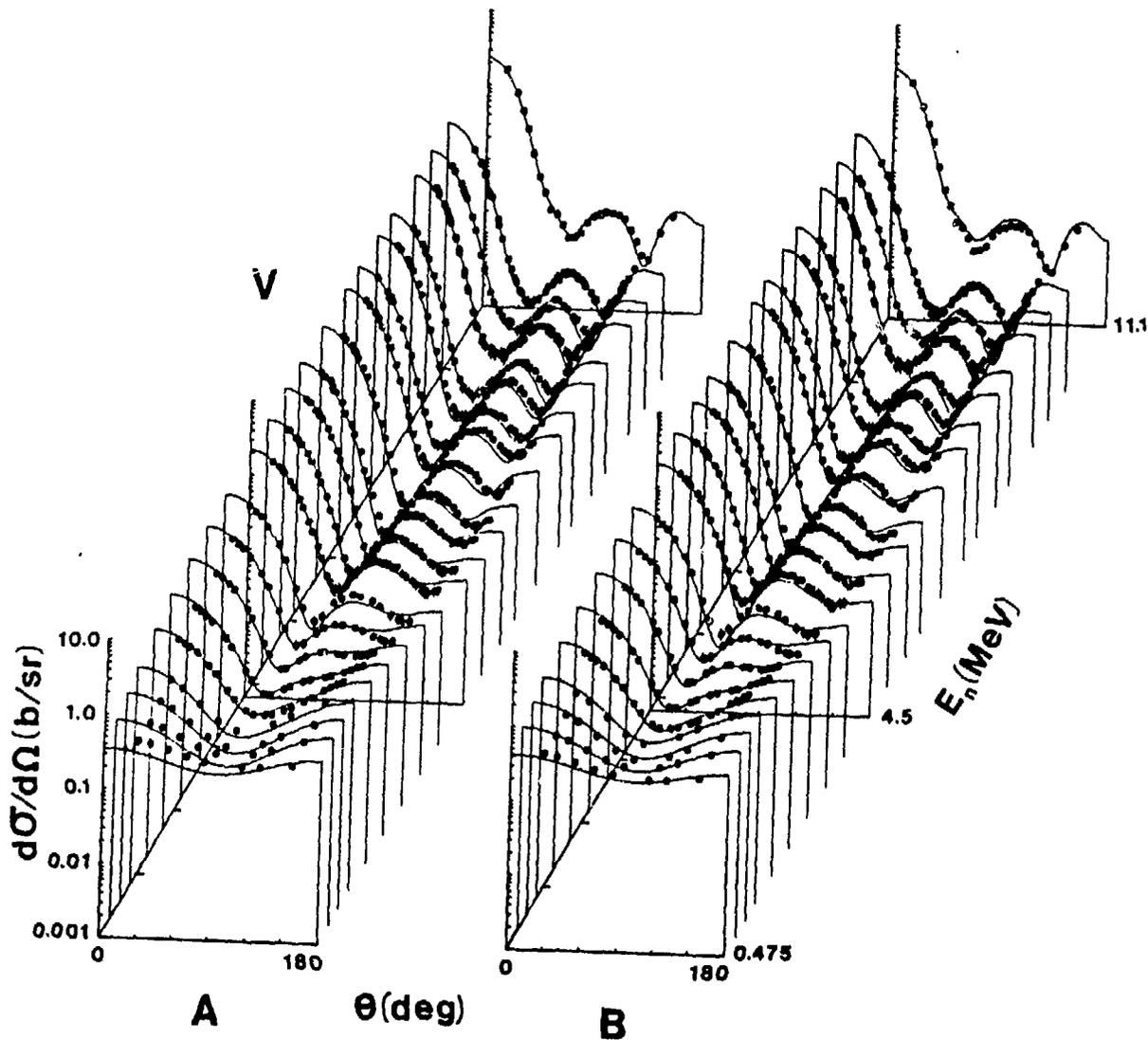
17

Fig. 5. Comparison of the experimental elastic angular distributions with those predicted by theory. Part-A shows the predicted results that arise when Eqs. (2) and (7) are used, whereas Part-B illustrates the predictions of the dispersion relationships, using Eqs. (2), (11), and (13) and the parameters of Table II. Throughout, data symbols indicate experimental values, and curves the calculated results. The data below 1.5 MeV are ≈ 300 keV averages of the low-energy results of Ref. 8. The data are given in the laboratory system.
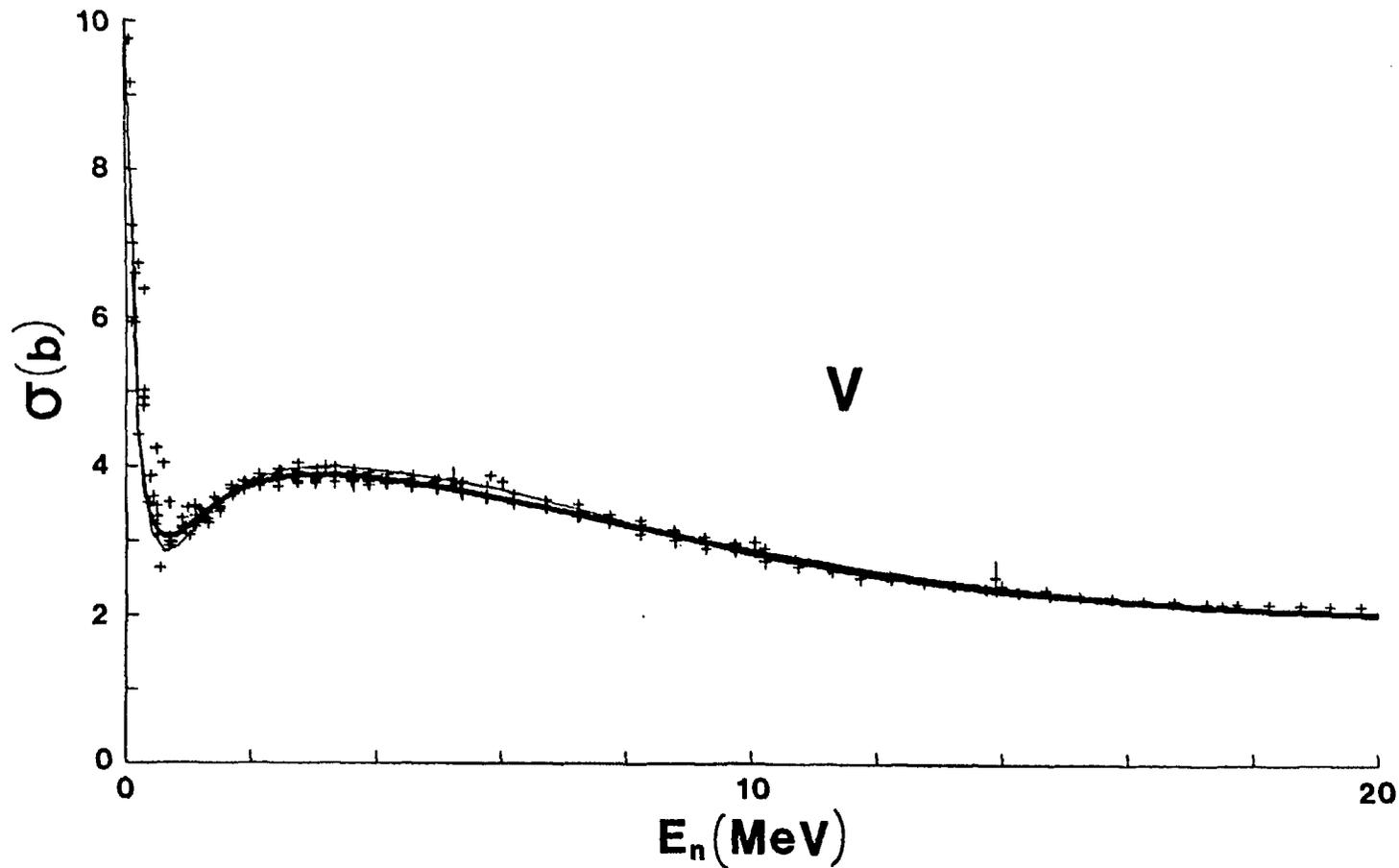
Fig. 6. Comparisons of calculated total cross sections of vanadium with broad energy-averages of the data base (symbols) available from the National Nuclear Data Center.[41] The light curve is the prediction made using Eqs. (2) and (7). The heavy curve is the result of employing Eq. (2) and the dispersion relationships (see Eqs. (11) and (13), together with Table II).

$$\langle r(E)^q \rangle_W = \frac{C_q (E - E_F)^2}{(E - E_F)^2 + D_q^2} , \qquad (11)$$

where C_q and D_q are constants to be fitted to the various moments of the imaginary potential. In addition, one expects $V_{HF}(r,E)$ to be a smooth function of the energy. Therefore, it is reasonable to approximate its moments by

$$\langle r(E)^q \rangle_{HF} = A_q + B_q E. \qquad (12)$$

When Eqs. (11) and (12) are substituted into Eq. (9), an analytic expression can be obtained for the various moments, $\langle r(E)^q \rangle_V$, of the total real potential,

$$\langle r(E)^q \rangle_V = A_q + B_q E + \frac{C_q D_q (E - E_F)}{(E - E_F)^2 + D_q^2} . \qquad (13)$$

The eighteen values of J_V, a_V, J_W, and a_W shown in Fig. 4, together with the OM radii given by Eq. (4), were used to calculate $\langle r(E)^q \rangle_V$ and $\langle r(E)^q \rangle_W$ when q = 0.8, 2.0, and 4.0. These were combined with the E = 0 moments obtained from the zero-energy limit of Eqs. (4) and (7), and for each of the three q-values, the parameters of Eqs. (11) and (13) were determined on the assumption that E_F = -9.68 MeV. The values obtained for these three quantities are listed in Table II.

If one now assumes that Eq. (13) holds for all values of E, and, further, takes V(r,E) to be a Woods-Saxon potential, the three moments of the interaction can be used to determine the strength and geometry, V_o, r_v, and a_v, for energies outside the 0.0 to 11.1 MeV region where the parameters A_q, B_q, C_q, and D_q were determined. In a similar manner, Eq. (11) can be used to find the values of W_o, r_w, and a_w under the assumption that the imaginary OM potential has a derivative Woods-Saxon shape. In this way one has an alternative to Eq. (7) for extrapolating the OM parameters to higher energies and, for the real potential, to bound states. This alternative gives rise to a smooth variation of the parameters over the entire energy range and, moreover, has some theoretical justification.

Table II. Constants Used in Evaluating Eq. (13)[a].

Constant	q = 0.8	2.0	4.0
A_q (MeV·fm^{q+1})	104.66	455.25	8372.9
B_q (fm^{q+1})	-0.721	-4.793	-114.3
C_q (MeV^{-1}·fm^{q+1})	13.49	87.67	2265.9
D_q (MeV)	8.05	6.9	5.95

a. Best-fit values for the various moments of the real and imaginary
    OM potentials when the parameterizations of Eqs. (11) and (13) are
    used.   The Fermi energy was taken to be -9.68 MeV in these
    considerations. The dimensions of the quantities are given in the
    first column of the table.

Figs. 7 and 8 show the results of applying the above approach to the real and imaginary OM potentials. The values of r_v and r_w calculated by use of Eqs. (13) and (11), respectively, are quite close to those given by Eq. (4), which were fixed before the final four-parameter fits to the data were made. The rms deviation of the former is 0.0014 fm, and the latter 0.0073 fm. For the real interaction, the quality of the fit to V_o and a_v is quite similar to that obtained by the use of Eq. (7). The rms deviations of V_o and a_v from the best four-parameter fits to the data are 0.83 MeV and 0.061 fm when Eq. (13) is used, compared to 0.70 MeV and 0.065 fm when Eq. (7) is taken. On the other hand, Eq. (7) gives a considerably better approximation to W_o and a_w than does Eq. (11). For the former, the rms deviation of these quantities from the best four-parameter fits is 1.79 MeV and 0.068 fm, while the latter gives 4.15 MeV and 0.117 fm. Despite this difference, the differential elastic-scattering cross sections predicted by the two different parameterizations are quite similar, as shown in Fig. 5. Neither, of course, gives as good a representation of the data as was obtained by the four-parameter fits shown in Fig. 1. However, at forward angles both fit the data quite accurately. It is only at back angles, where the cross section is small and detailed shape becomes important, that they deviate appreciably from experiment. The one exception to this is at 11.1 MeV where the depth of the first minimum predicted by the dispersion relations is $\approx$ 13 mb, which is 35% larger than the 9.5 mb reported by Ferrer et al.[10] Also shown in Fig. 5 are 300 keV averages of the experimental results of Smith et al[8] for energies extending from 0.3 to 1.5 MeV. Either OM parameterization gives a fair prediction of these low-energy averaged data.

In Fig. 6 the total cross section predicted using the dispersion-relationship approach (heavy curve) and the results obtained with Eq. (7) (light curve) are compared with the experimental data. In the 0.5 to 1.0 MeV region, Eq. (7) gives a somewhat deeper minimum and may be in better agreement with experiment. Between 3.0 and 6.0 MeV the dispersion-relation predictions are slightly better than those obtained with Eq. (7), while in the 10.0 to 14.0 MeV range the roles of the two parameterizations are interchanged. Above 14.0 MeV the two give almost identical results. Finally, the ℓ = 0 strength function predicted by Eqs. (11) and (13), S_o = 5.76 x 10^{-4}, is somewhat smaller than the value deduced from resonance experiments,[42] S_o = (7.7 ± 1.2) x 10^{-4}. Thus, in the energy range 0.0 to 20.0 MeV, either parameterization gives an adequate prediction for the total cross section with perhaps the low-energy data showing a small preference for Eq. (7).
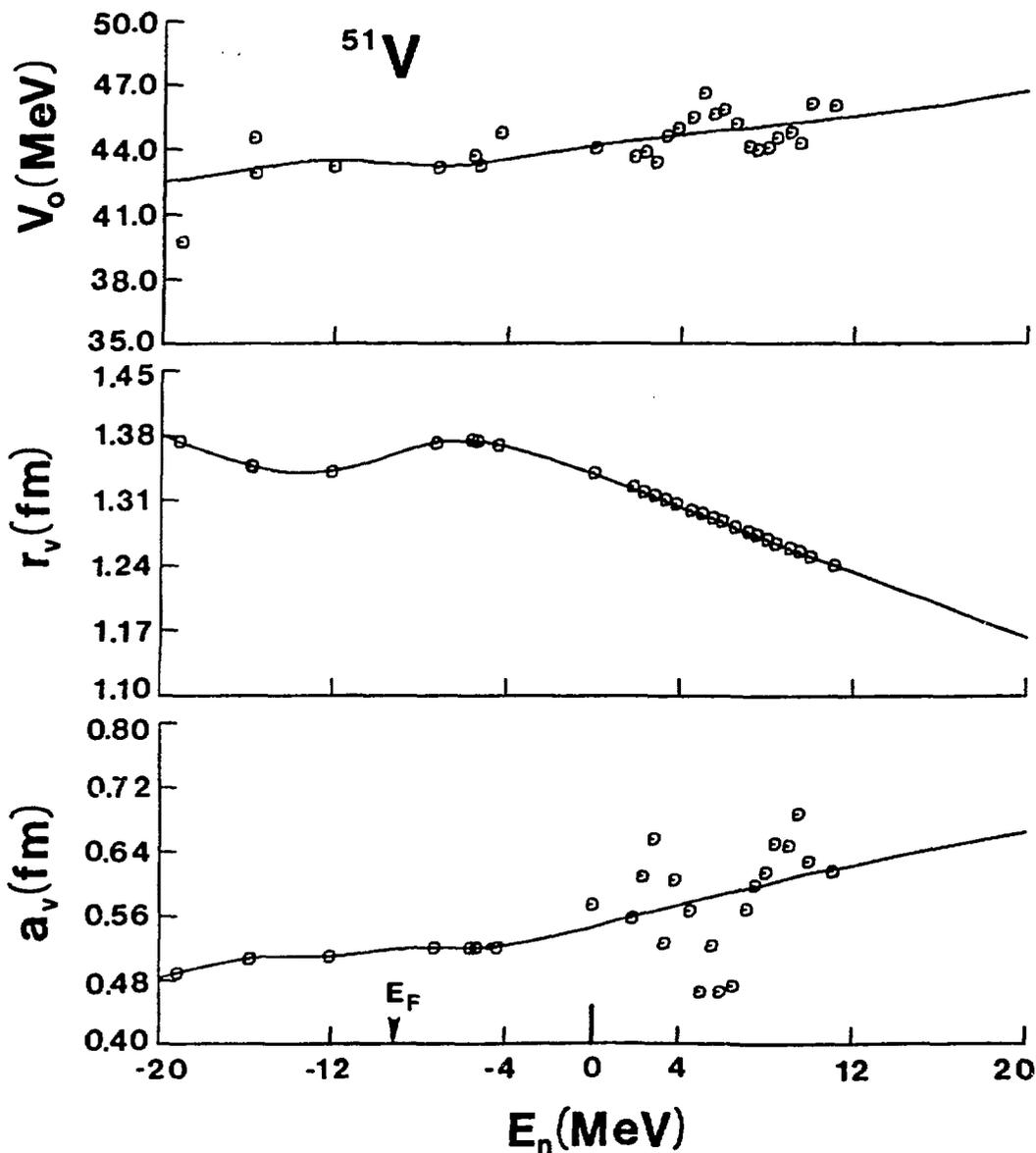
Fig. 7. The solid lines are the predicted variation with energy of V_o, r_v, and a_v for a Woods-Saxon potential. These result when the $q = 0.8$, 2, and 4 moments of the real potential, obtained from the best four-parameter fit to the experimental data, are approximated by Eq. (13). The 0's at positive energies are the values obtained from the experimental fitting of the scattering data. The same symbols for $E < 0$ indicate the magnitudes of V_o needed to fit the binding energies of particle- and hole-states when r_v and a_v have the values predicted by Eq. (13). In order of increasing binding energy, the bound states are: $0g_{9/2}$, $1p_{1/2}$, $0f_{5/2}$, $1p_{3/2}$, $0f_{7/2}$, $1s_{1/2}$, $0d_{3/2}$, and $0d_{5/2}$. The first four are particle states and the last four, hole states. $E_F = -9.68$ MeV is also shown.

23

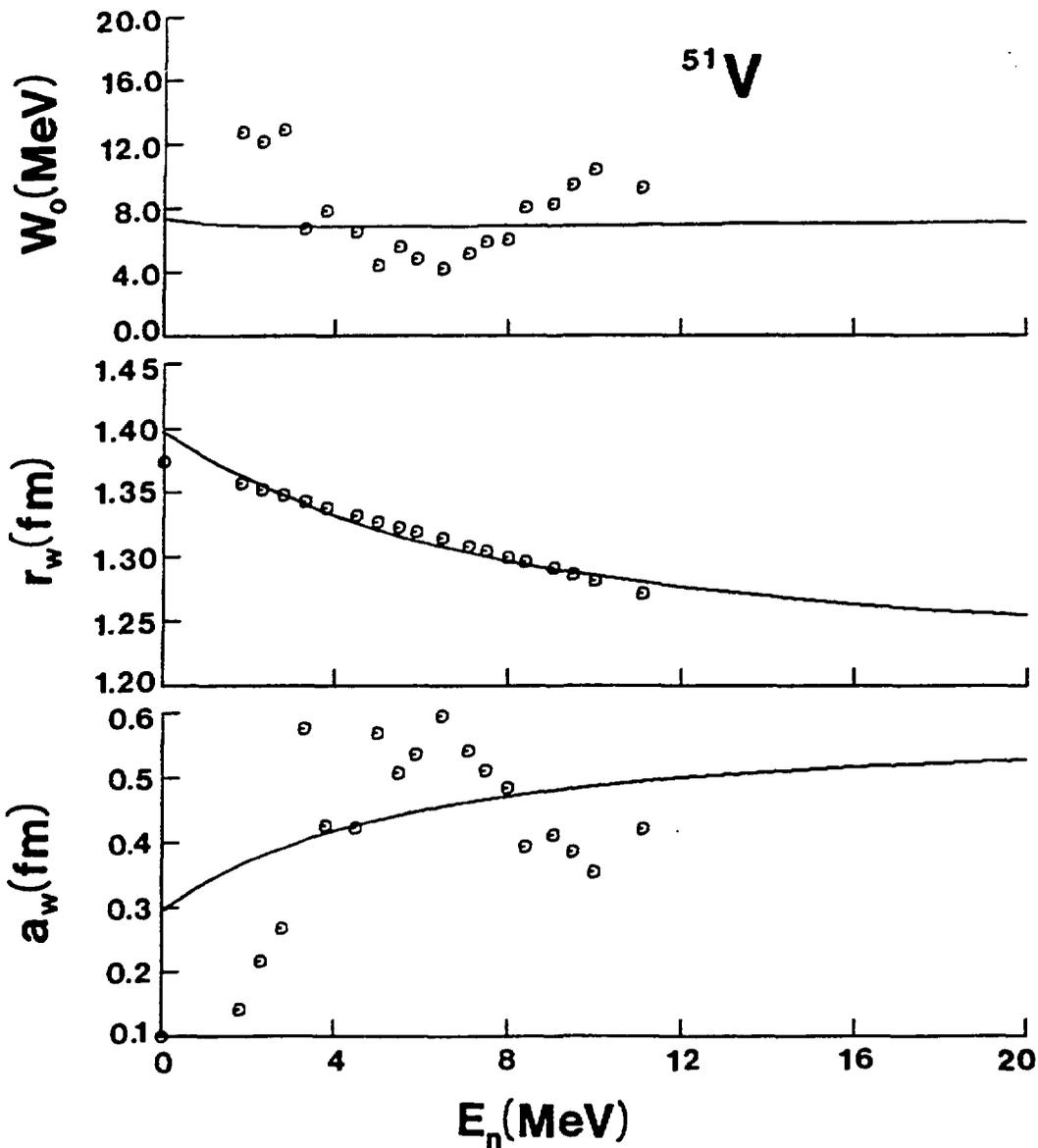Fig. 8. The solid lines are the predicted variation with energy of W_o, r_w, and a_w for a derivative Woods-Saxon well. These result when the $q = 0.8$, 2, and 4 imaginary-potential moments of the best four-parameter fit to the experimental scattering data are approximated by Eq. (11). The O symbols indicate the respective values obtained from the fitting. The experimental value of W_o at $E = 0$ (not shown) is 20.7 MeV.

Fig. 9 shows the J_v values as a function of energy predicted by Eq. (13) when the q = 2 values of Table II are used. For E > 0, J_v is indistinguishable from a straight line, and the values of this quantity, extracted from the four-parameter fits to the scattering data (indicated by O's), are seen to cluster about the predicted curve with an rms deviation of 8.7 MeV-fm^3. For E < 0, J_v is non-linear and reaches a peak at about -6.0 MeV. It then turns over and reaches a minimum at $\approx$ -13.5 MeV, before beginning to rise again. In order to check the predicted form of J_v for negative energies, one must look at values of this quantity necessary to reproduce the observed single-particle and single-hole energies. However, the definition of these quantities is ambiguous when one deals with a non-closed-shell core. For example, when the $1p_{3/2}$ neutron binds to the $7/2^-$ ground state of ^{51}V, the spins can couple to I = 2^+, 3^+, 4^+, and 5^+. If these states are widely separated in energy it is not clear what to accept as the single-particle energy. In actual fact, in ^{52}V candidates for all four of these states lie within 150 keV of the ground state.[47] Thus, the simple approximation in which one takes the difference between the binding energy[48] of ^{52}V and ^{51}V, -7.311 MeV, differs only slightly from the average binding energy of the four states, -7.264 MeV. On the other hand, the energy to be taken for the $f_{7/2}$ neutron-hole state is ambiguous since the $f_{7/2}$ nucleon can couple to the ^{51}V ground state to give I = 7^+, 6^+, 5^+, 4^+, 3^+, 2^+, 1^+, and 0^+. Candidates for the first seven of these states lie within 1.35 MeV of the ^{50}V ground state,[49] whereas the I = 0^+ is a T = 3 level, located at 4.805 MeV, and is the isobaric analog of the ^{50}Ti ground state. If one simply takes the binding energy difference between ^{50}V and ^{51}V, one would conclude that $\epsilon_{f_{7/2}}$ = -11.051 MeV, while the average over the yrast I = 0^+ to 7^+ states gives -12.093 MeV. In either case the value of J_v needed to give the binding energy for the $f_{7/2}$ level is smaller than the analogous quantity for the $p_{3/2}$ state, and this is predicted by Eq. (13), as shown in Fig. 9. The binding energies shown by the O's in this figure are those that arise when the average over the yrast states is taken. In this way one concludes that the Fermi energy, E_F, is $1/2 \cdot (\epsilon_{f_{7/2}} + \epsilon_{p_{3/2}})$ = -9.68 MeV.
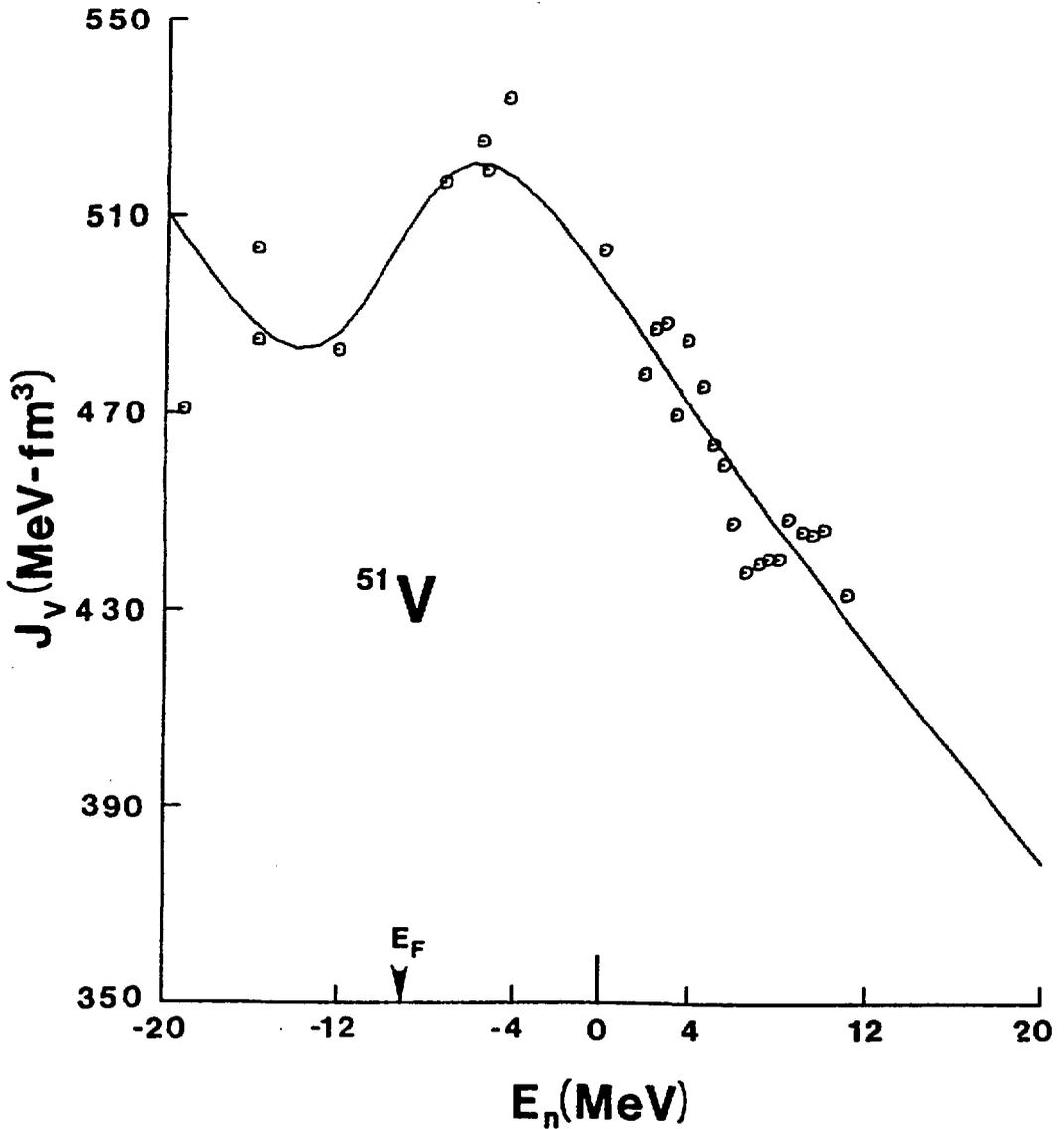
Fig. 9. The solid line shows the values of J_v predicted by the use of Eq. (13) with q = 2 and the parameters given in Table II. The O symbols indicate experimentally derived values of this quantity, as further defined in the caption of Fig. 7.

The energies of the other particle and hole states, shown in Fig. 9, were estimated in the following manner: From the ^{48}Ca(d,p)^{49}Ca stripping data,[50] the single-particle energies of the $1p_{1/2}$, $0f_{5/2}$, and $0g_{9/2}$ levels can be obtained, while the $1s_{1/2}$, $0d_{3/2}$, and $0d_{5/2}$ hole-state energies can be gotten from the ^{48}Ca(p,d)^{47}Ca pick-up results.[51] These, of course, give the binding energies relative to the ^{48}Ca core, and in order to translate these to ^{51}V, one must know what influence the addition of three $f_{7/2}$ protons has on these numbers. This was estimated for each of the states by making a shell-model calculation in which the proton-proton interaction was the one that best reproduced the spectra[7] of ^{50}Ti, ^{51}V and ^{52}Cr, and the proton-neutron matrix elements were calculated using the Schiffer-True potential.[52] In this way, for example, the diagonalized states of the $(\pi f_{7/2})^3(\nu s_{1/2})$ configuration were calculated, and the additional binding due to the three $f_{7/2}$ protons was determined from the average energy of the yrast 3^- and 4^- states. The energy values shown in Fig. 9 (other than those for the $1p_{3/2}$ and $0f_{7/2}$ states) were obtained in this way.

In order to estimate the value of J_v needed to reproduce these binding energies, a_v and r_v were held fixed at the values given by Eq. (13), and V_o, the Woods-Saxon depth, was varied so as to reproduce the desired energy when the spin-orbit interaction of Eq. (2) was assumed. Clearly, as can be seen from Fig. 9, the values of J_v required to obtain the hole- and particle-state binding energies bear out the trend predicted by the dispersion relations.

VI. DISCUSSION

A comprehensive data base describing the neutron interaction with vanadium was interpreted in terms of the spherical optical-statistical model. The use of the spherical OM is justified by the following:

(i)   Measured inelastic-scattering cross sections to states below
        $\approx$ 2.6 MeV agree well with the predictions of a spherical OM
        and Hauser-Feshbach theory,[37] as modified by Moldauer[39] (see
        Fig. 3). There is no evidence for an appreciable direct-
        reaction component.

(ii) For the closed-shell-plus-one nuclei ^{89}Y and ^{209}Bi, J_w at E = 0 has the values 66.47 and 33.87 MeV-fm^3, respectively.[53,1] The value for ^{51}V, J_w = 53 MeV-fm^3, lies between these and increases with increasing energy, as would be expected physically. (This is in contrast to the deformed nucleus ^{59}Co, where J_w at E = 0 is more than twice as large, 135 MeV-fm^3, and decreases with increasing energy.[6])

(iii) In a study of low-energy neutron scattering from Z = 39 to 51 nuclei, it was found that r_w for deformed nuclei is smaller than r_v, whereas for spherical nuclei $r_w > r_v$.[54] The spherical fit to ^{51}V leads to $r_w > r_v$. (In Ref. 6 it was shown that a decrease in r_w occurs when one attempts to fit pseudo-scattering data generated with a deformed potential using a spherical OM.)

(iv) The $(\pi f_{7/2})^3$ spherical shell model predicts the low-lying excited states of ^{51}V extremely well.[7]

        With nuclei as light as ^{51}V, one encounters difficulties in determining the optimum OM parameters for several reasons. First, fluctuations are in evidence, even at E = 5.0 MeV, and they require that the data be averaged over fairly wide energy intervals in order to obtain an experimental cross section consistent with that implied by the OM. Below 4.0 MeV the energy-averaging interval in the present work was ≈ 500 keV. It is clear that compound-nucleus contributions change over such an averaging interval as prominent channels open, leading to uncertainties in the resulting OM parameters. Furthermore, even at the highest energies of the present work, the elastic-scattering angular distributions are rather structureless compared to those observed in heavier nuclei or at higher energies, and this inhibits good definition of OM parameters. Despite these problems, it was found, after some initial calculations, that r_v and r_w varied rather smoothly with energy and could be described by the values given in Eq. (4). The remaining four parameters, the real and imaginary strengths and diffusenesses, were then varied to give the best fit to the data shown in Fig. 1. The values of the resulting parameters had considerable spatter, as shown in Fig. 4, particularly for the imaginary potential at energies below 4.0 MeV. The energy averages of the data at 3.3 and 3.8 MeV lead to

$a_w \approx 0.5$ fm and a rather large $J_w \approx 90$ MeV-fm^3. On the other hand, the fit to the three low-energy averaged cross sections implies smaller a_w values and, for the 1.8 and 2.3 MeV distributions, smaller J_w values. Thus, below 4.0 MeV where fluctuations are extremely important, the fitting gives conflicting imaginary-potential properties, and it is only when one considers the neutron total cross sections in the 0.5 to 1.0 MeV range that one finds the smaller a_w and J_w values are needed to reproduce the observed dip in the total cross section shown in Fig. 6.

If the spatter in the OM parameters is smoothed according to Eq. (7), one obtains the predicted angular distributions shown in Fig. 5A. Although the agreement with observations is not as good as the best four-parameter fit of Fig. 1, the description is reasonably suitable and, furthermore, the predictions agree fairly well with the broad energy averages of data below 1.5 MeV obtained at this laboratory many years ago.[8] Eq. (7) gives an S_0 strength function of 7.24×10^{-4}, in excellent agreement with the value deduced from resonance measurements,[42] $(7.7 \pm 1.2) \times 10^{-4}$. The total cross section predicted by this parameterization is indicated by the light curve in Fig. 6, and over the entire energy range, 0 to 20.0 MeV, the prediction is within $\approx 3\%$ of the experimental values. The important characteristics of this parameterization are: a_w is small for $E \to 0$, a_v is essentially energy independent, and the rapid energy dependencies of r_v and r_w disappear above ≈ 10.0 MeV. Furthermore, above ≈ 6.0 MeV, dJ_v/dE changes from -8.3 to -2.9 fm^3. The latter value is in good agreement with the global results of Rapaport[2], -2.74 fm^3, or Walter and Guss[3], -2.82 fm^3, both of which were obtained from the analysis of high-energy neutron-scattering data.

An alternate smooth representation of the OM potential is provided by the dispersion relationship[16] which relates the total real potential to its Hartree-Fock component, plus a principal-value integral, over energy, of the imaginary interaction. As discussed in the previous section, various radial moments of the real and imaginary interaction are also related, and if one smooths the values of $<r^q>_w$ by use of Eq. (11) for $q = 0.8$, 2.0, and 4.0, one obtains the W_0, r_w, and a_w for the derivative Woods-Saxon imaginary potential shown in Fig. 8. The analogous quantities for the real Woods-Saxon well obtained from Eq. (13) with the parameters of Table II are shown in Fig. 7. The value of r_v obtained in this way does not decrease as markedly with increasing

binding energy as that given by Mahaux and Sartor for ^{208}Pb,[12,13] for ^{89}Y,[14] and for ^{40}Ca.[15] The origin of this difference was examined, and it was found that it is, in part, a consequence of not considering the higher-energy scattering data. For example, if the global potential of Walter and Guss[3] is used to generate an additional nineteen sets of differential cross sections, ranging from 12.0 to 30.0 MeV in 1.0 MeV steps, r_v reaches its maximum at -3.0 MeV rather than the -6.0 MeV shown in Fig. 7. Moreover, in the region 0 to -20.0 MeV, the difference between the minimum and maximum values of r_v increases from the 0.04 fm shown in Fig. 7 to 0.08 fm. Thus, the magnitude of the dip in r_v as one approaches E_F is extremely sensitive to the high-energy behavior of the potential.

When the dispersion relations are solved using the parameters of Table II, the differential elastic-scattering distributions shown in Fig. 5B are obtained. These values are quite similar to the results obtained using Eq. (7), except for the 11.1 MeV distribution where the predictions of Eq. (7) are somewhat better. The total cross sections predicted with Eqs. (11) and (13) (heavy curve of Fig. 6) are quite similar to those obtained with Eq. (7), and are in good agreement with experiment. The S_0 strength function is predicted to be 5.76 x 10^{-4}, in fair agreement with the value deduced from resonance measurements,[42] (7.7 ± 1.2) X 10^{-4}.

Consider now the problem of the bound states. As stated in the previous section, when a nucleon or hole is bound to a non-closed-shell core, the definition of the single-particle energy is not clear-cut. In the present work the single-particle or hole energy was somewhat arbitrarily defined as the average over all the spin states attainable by coupling the particle or hole to the $J^{\pi} = 7/2^-$ ground state of ^{51}V, instead of taking it to be the binding energy of the yrast level. For the $p_{3/2}$ state this makes little difference, since the four possible spin states are almost degenerate. On the other hand, for the $f_{7/2}$-hole state the averaging procedure increases the binding energy by $\approx$ 1.0 MeV. The numerical values in these two cases, obtained directly from the experimental binding-energy tables,[48] together with the spectra of ^{52}V,[47] and ^{50}V,[49] are shown in Fig. 9. However, for the other particle- and hole-states the situation is more complicated, since the experimental positions of the various multiplets in ^{52}V and ^{50}V are unknown. If r_v and a_v were constants for negative energies, the values

of V_0 needed to give the binding energies appropriate to the particle states in ^{49}Ca,[55] and the hole states in ^{47}Ca,[56] could be determined and these then translated to the values of J_v required for these states in ^{51}V by using, for example, the Rapaport[2] global change in the potential depth, $-22.7(N-Z)/A$ MeV, and an appropriate increase in the well radius governed by $R_v = r_v A^{1/3}$. However, according to Fig. 7, both r_v and a_v depend on energy. Thus, the procedure used for determining the "experimental" values for the single-particle energies of the other particle- and hole-states was to take the energies of the $0d_{5/2}$, $0d_{3/2}$, and $1s_{1/2}$ holes[56] in ^{47}Ca, and the $1p_{1/2}$, $0f_{5/2}$ and $0g_{9/2}$ states[55] in ^{49}Ca, and to estimate the extra binding due to the three additional $f_{7/2}$ protons by a shell-model calculation, as described in the previous section. The values of J_v needed to obtain these binding energies are shown in Fig. 9, and the results are in close agreement with those predicted by the use of the dispersion relationship.

One might, of course, question the use of the shell model to give "experimental" binding energies of particle and hole states in ^{51}V. One can examine how closely the single-particle and hole energies in ^{49}Ca and ^{47}Ca, together with the shell-model calculations, reproduce the observed energies of these states in ^{57}Ni and ^{55}Ni. For the $1p_{1/2}$, $0f_{5/2}$ and $0g_{9/2}$ states, the shell-model calculation gives -9.07, -9.93, and -8.14 MeV, respectively, whereas the experimental values in ^{57}Ni,[48,57] are -9.17, -9.51 and -7.26 MeV. Thus, one would expect that, in ^{51}V where the added neutron interacts with three $f_{7/2}$ protons instead of eight, the predicted binding energy for the $1p_{1/2}$ state would be quite accurate, while for the $0f_{5/2}$ and $0g_{9/2}$ levels it would be, respectively, $\approx$ 200 and 400 keV too large. From an inspection of Fig. 9, it is clear that the value of J_v needed to give the "correct" binding of the $p_{1/2}$ level is almost identical to the dispersion-relationship value, while for the $0f_{5/2}$ and $0g_{9/2}$ levels it is, respectively, greater by 0.88% and 2.93%. (If the required binding energies of the $0f_{5/2}$ and $0g_{9/2}$ levels are reduced by 200 and 400 keV, respectively, these percentages become 0.22% and 1.79%. Similarly, in ^{55}Ni the positions of the $(1s_{1/2})^{-1}$ and $(0d_{3/2})^{-1}$ levels are probably known and the binding

energies[48,58] are -19.80 and -20.37 MeV, while shell-model calculations give -19.73 and -22.64 MeV for the two corresponding values. Thus, the prediction of the $(1s_{1/2})^{-1}$ level is in excellent agreement with experiment, but for the $(0d_{3/2})^{-1}$ level in ^{51}V, the shell-model estimate probably gives $\approx$ 700 keV too much binding. Again the results are in agreement with those shown in Fig. 9, as the $s_{1/2}$ hole has a J_v value almost identical to the dispersion-relationship prediction, while the $(0d_{3/2})^{-1}$ hole value is 3.24% larger than given by Eq. (13). (If the $d_{3/2}$ hole energy is 700 keV less tightly bound, this discrepancy is reduced to 1.38%.) In all cases it is clear that the values of J_v needed to give the observed binding energies follow quite closely the dispersion-relationship predictions.

Because of the dispersion relationship, Eq. (8), it seems clear that the concept of a global OM does not have validity, particularly at low energies. The imaginary potential is supposed to account for the effects of those levels not explicitly considered in the OM calculations. Since there are fewer low-lying states in an even-even nucleus, the imaginary potential should be different for adjacent even-even and odd-even nuclei. The same is also true for neighboring odd-even nuclei. For example, ^{51}V has a closed N = 28 neutron shell, and below $\approx$ 2.7 MeV has only eight excited states--five of them accounted for by various couplings of the $(\pi f_{7/2})^3$ configuration.[7] On the other hand, ^{53}V, which has two neutrons outside the N = 28 shell, has eighteen states in this excitation range.[59] Thus, one would expect the imaginary potential to vary from nucleus to nucleus, and because the principal-value integral of Eq. (8) involves the surface-imaginary potential, the real interaction should have r_v and a_v values dependent on the nucleus in question. The degree to which this variation in OM parameters is a concern will depend, of course, on the accuracy with which one wishes to describe the experimental data.

VII. CONCLUSIONS

In summary, the main conclusions of this study are:

(a)   Spherical OM Interpretation   The elastic neutron scattering and the neutron total cross section, together with inelastic excitations below $\approx$ 2.6 MeV, of vanadium can be understood in terms of the spherical optical-statistical model. An adequate approximation of this potential, particularly for applied work, is given by either Eq. (7) or the dispersion

relationships of Eqs. (11) and (13), together with the parameters of Table II. The very low-energy data favors the parameterization of Eq. (7).

(b) $\underline{J_v\ vs\ E\ curve\ 16.0\ to\ 20.0\ MeV\ above\ E_F}$ From Fig. 4 and Eq. (7), it is clear that near 6.0 MeV (i.e., $\approx$ 16.0 MeV above E_F) the slope of J_v changes from $dJ_v/dE \approx -8.3$ fm^3 to ≈ -2.74 fm^3. The latter is similar to the global values. Such a change in slope has been noticed in the analysis of the ^{209}Bi data[1] (where it was found to occur $\approx$ 15.5 MeV above E_F) and in a ^{59}Co analysis[6] (where the transition occurs $\approx$ 19.5 MeV above E_F). This change marks a transition between low- and high-energy results, and is probably a manifestation of the onset of the Fermi surface anomaly.

(c) $\underline{Low-/high-Energy\ Dichotomy}$ From a study of the strength function, low-energy neutron scattering data and polarization data, Moldauer[60] concluded that a_w was small and r_v was greater than 1.26 fm for all but the transuranic elements. Similar values of r_v and a_v have been found in the analysis of ^{59}Co and ^{209}Bi data.[1,6] The present ^{51}V results are another example of this behavior. These values are in contrast to those of global models. These conclusions, combined with those cited in (b), above, imply that great care must be taken in extrapolating between low- and high-energy OM parameters.

(d) $\underline{Fermi\ Surface\ Anomaly}$ Mahaux and Ngo[61] have predicted a flattening out of J_v, and then a change in sign of dJ_v/dE, near $E \approx 0$. This effect is known as the Fermi surface anomaly. From Figs. 4 and 9 it is evident that for $E > 0$ the scattering data do not indicate more than a linear energy dependence of J_v in the range $0 \leq E \leq 6.0$ MeV. However, the values of J_v needed to reproduce the single-particle and hole bound-state energies exhibit this anomaly. Indeed, J_v quite closely follows the dispersion-relationship curve predicted by Eq. (13) and the parameters of Table II. Thus clear evidence of the Fermi surface anomaly is found, but only from an analysis of bound-state data.

(e) $\underline{Method\ of\ Moments\ and\ the\ Extrapolation\ of\ OM\ Parameters}$ The various radial moments of the real and imaginary OM potential have been parameterized in terms of Eqs. (11) and (13). The parameters (A_q to D_q, see Table II) have been determined by

fitting the data at nineteen energies between 0 and 11.1 MeV, and they have been used to deduce the OM interaction in the region $-20.0 \leq E \leq 20.0$ MeV. It was found that results in good agreement with experimental values could be obtained for both $E < 0$ (see Fig. 9) and for $E > 0$ (see Figs. 5B and 6). Although the extrapolation gives a good account of the data, the predicted values of r_V and V_0 do not show the marked structure reported by Mahaux and Sartor[12-15] for the nuclei ^{208}Pb, ^{89}Y and ^{40}Ca when $E < 0$. These authors found that r_V decreases and V_0 increases with increasing binding energy. It is clear (see Fig. 7) that for $E < 0$, V_0 certainly does not become larger with binding energy, and r_V shows a very weak dependence on E. It was found that a large part of this difference in behavior is due to the neglect of the $E > 11.1$ MeV data in deducing the parameters of Table II. Thus, even though an adequate extrapolation of the OM potential can be obtained using only the 0 to 11.1 MeV results, the neglect of the higher-energy data may lead to unphysical properties for V_0 and r_V.

(f)   <u>Global OM Potential</u> Because the imaginary potential describes the contributions of channels neglected in the OM analysis, this quantity should vary from nucleus to nucleus, and there should certainly be a different behavior for even-even and odd-even nuclei. Furthermore, because of the dispersion relationship of Eq. (8), the real potential should also be a function of the nucleus in question. This should be particularly true for r_V and a_V at low energies because of the surface nature of the imaginary potential. However, at higher energies, the number of neglected channels is so large that any differences in the low-lying states of the target nuclei are probably insignificant, and the concept of the global OM may become once more valid. The accuracy with which one seeks to describe the experimental data will determine to what extent the use of a global OM is suitable at low energies.

REFERENCES

[1] R. D. Lawson, P. T. Guenther and A. B. Smith, Phys. Rev. C36 1298 (1987), the energy variation of J_w given in Eq. (6) of this paper should be +(1.05 ± 0.37)E.

[2] J. Rapaport, Phys. Reports 87 25 (1982).

[3] R. L. Walter and P. P. Guss, Proc. Conf. on Nucl. Data for Basic and Applied Science, edited by P. Young, R. Brown, G. Auchampaugh, P. Lisowski, and L. Stewart, vol. 2, p. 1079 (Gordon and Breach, New York, 1986).

[4] P. T. Guenther A. B. Smith, and J. F. Whalen, Nucl. Sci. and Eng. 82 408 (1982).

[5] A. B. Smith, P. T. Guenther, D. Smith, and J. F. Whalen, Nucl. Sci. and Eng. 72 293 (1979).

[6] A. B. Smith, P. T. Guenther, and R. D. Lawson, Nucl. Phys. A, in press.

[7] R. D. Lawson, Theory of the Nuclear Shell Model (Clarendon, Oxford, 1980).

[8] A. Smith, J. Whalen, and K. Takeuchi, Phys. Rev. C1 581 (1970).

[9] P. Guenther, D. Havel, A. Smith, and J. Whalen, Nucl. Sci. and Eng. 64 733 (1977).

[10] J. Ferrer, J. Carlson, and J. Rapaport, Nucl. Phys. A275 325 (1977).

[11] A. B. Smith, P. T. Guenther, D. L. Smith, J. W. Meadows, R. J. Howerton, and T. Jemiel, Argonne National Laboratory Report ANL/NDM-105, to be published.

[12] C. Mahaux and R. Sartor, Phys. Rev. Lett. 57 3015 (1986).

[13] C. Mahaux and R. Sartor, Nucl. Phys. A468 193 (1987).

[14] C. Mahaux and R. Sartor, Phys. Rev. C36 1777 (1987).

[15] C. Mahaux and R. Sartor, to be published.

16 G. R. Satchler <u>Direct Nuclear Reactions</u> (Clarendon, Oxford, 1983).

17 C. Budtz-Jorgensen, P. Guenther, A. Smith, J. Whalen, W. McMurray, M. Renan, and I. Van Heerden, Z. Phys. <u>319</u>, 47 (1984).

18 A. Smith, P. Guenther, J. Whalen, I. van Heerden, and W. McMurray, J. Phys. <u>G11</u>, 125 (1985).

19 P. Guenther, A. Smith, and J. Whalen, Phys. Rev. <u>C12</u>, 1797 (1976).

20 A. Smith, P. Guenther, R. Larson, C. Nelson, P. Walker, and J. Whalen, Nucl. Intr. and Methods <u>50</u>, 277 (1967).

21 A. Smith, P. Guenther, and R. Sjoblum, Nucl. Instr. and Methods <u>140</u>, 397 (1977).

22 <u>Nuclear Standards File</u> IAEA Tech. Report 227, editors H. Conde, A. Smith and A. Lorenz, IAEA Press, Vienna (1983).

23 P. T. Guenther, <u>The Scattering of Fast Neutrons from the Even Isotopes of Tungsten</u> Thesis, University of Illinois (1977).

24 Zhou Chunmei, Zhou Enchen, Lu Xiane, and Hou Junde, Nuclear Data Sheets <u>48</u> 111 (1986).

25 F. Perey and W. Kinney, Oak Ridge National Laboratory Report, ORNL-4551 (1970).

26 J. Towle, Proc. Conf. on Study of Nuclear Structure with Neutrons, North-Holland Pub. Co., Amsterdam (1966), paper 37.

27 B. Holmqvist and T. Wiedling, Aktiebolaget Atomenergi Reports, AE-385 (1970) and AE-430 (1971).

28 D. L. Smith, Private Communication (1975), Data available at the National Nuclear Data Center, Brookhaven National Laboratory.

29 E. Alman and E. Ramstrom, Aktiebolaget Atomenergi Report, AE-503 (1975).

30 T. Holmqvist, S. Johansson, G. Lodin, and T. Wiedling, Nucl. Phys <u>A146</u> 321 (1970).

31 P. Buchanan et al., Texas Nucl. Corp. Report, ORO-2791 (1967), Data available from the National Nuclear Data Center, Brookhaven National Laboratory.

32 A. Barrows, R. Lamb, D. Velkley, and M. McEllistrem, Nucl. Phys. A107 153 (1968).

33 D. Porter, R. Coles, and W. Gilboy, AWRE Report, AWRE-0-78/70 (1970).

34 L. Cranberg and J. Levin, Phys. Rev. 103 343 (1956).

35 H. Feshbach, C. Porter, and V. Weisskopf, Phys. Rev. 96 448 (1954).

36 P. E. Hodgson, Nuclear Reactions and Nuclear Structure (Clarendon, Oxford, 1971).

37 W. Hauser and H. Feshbach, Phys. Rev. 87 366 (1952).

38 A. B. Smith, P. T. Guenther, J. F. Whalen, and R. D. Lawson, Argonne National Laboratory Report, ANL/NDM-101 (1987); see also Ref. 6.

39 P. A. Moldauer, Nucl. Phys. A344 185 (1980).

40 ABAREX, A Spherical Optical Model Code, P. A. Moldauer, Private communication (1983), and as revised by R. D. Lawson (1986).

41 National Nuclear Data Center, Brookhaven National Laboratory.

42 S. F. Mughabghab, M. Divadeenam, and N. E. Holden, Neutron Cross Sections Vol.-1, Part-A (Academic, New York, 1980).

43 CINDA Index to the literature and computer files on microscopic neutron data, IAEA Press Vienna (1987).

44 M. Mackwe et al., Phys. Rev. 114 1563 (1959).

45 S. Cox and E. Cox, Argonne National Laboratory Report, ANL-7935 (1972).

46 A. Gilbert and A. Cameron, Can. Jour. Phys. 43 1446 (1965).

47 J. R. Beene, Nucl. Data Sheets 25 235 (1978).

[48] A. H. Wapstra and K. Bos, Atomic Data and Nucl. Data Tables **19** 177 (1977).

[49] D. E. Alburger, Nucl. Data Sheets **42** 369 (1984).

[50] T. W. Burrows, Nucl. Data Sheets **48** 569 (1986).

[51] T. W. Burrows, Nucl. Data Sheets **48** 1 (1986).

[52] J. P. Schiffer and W. W. True, Rev. Mod. Phys. **48** 191 (1976).

[53] R. D. Lawson, P. T. Guenther, and A. B. Smith, Phys. Rev. **C34** 1599 (1986).

[54] A. B. Smith, P. T. Guenther, and J. F. Whalen, Nucl. Phys. **A415** 1 (1984).

[55] T. W. Burrows, Nucl. Data Sheets **48** 569 (1986).

[56] T. W. Burrows, Nucl. Data Sheets **48** 1 (1986).

[57] T. W. Burrows and M. R. Bhat, Nucl. Data Sheets **47** 1 (1986).

[58] Zhou Enchen, Huo Junde, Zhou Chunmei, Lu Xiane, and Wang Lizheng, Nucl. Data Sheets **44** 463 (1985).

[59] L. K. Peker, Nucl. Data Sheets **43** 481 (1984).

[60] P. A. Moldauer, Nucl. Phys. **47** 65 (1963).

[61] C. Mahaux and H. Ngo, Nucl. Phys. **A378** 205 (1982); Phys. Lett. **B100** 285 (1981).